J. Fluid Mech. (1987), *vol.* 179, *pp.* 227–252
Printed in Great Britain

The resonant-triad nonlinear interaction in boundary-layer transition

By F. T. SMITH† AND P. A. STEWART
Department of Mathematics, University College London, Gower Street, London WC1E 6BT, UK.

(Received 22 April 1986 and in revised form 30 August 1986)

Recent controlled experiments by Kachanov & Levchenko (1984) and others indicate that, during some slower kinds of transition to turbulence in boundary layers, three-dimensionality can come into play initially as a resonant-triad phenomenon, depending on the disturbance sizes present. The triad interaction, suggested theoretically in the boundary-layer context by Craik (1971) and others, is studied in the present work by means of multi-structured analysis for high characteristic Reynolds numbers. A finite-amplitude/relatively high-frequency approach leads rationally to the nonlinear triad equations, solutions for which are then obtained analytically and computationally in certain central cases of interest (temporal and spatial). The solutions have a rather chaotic spiky appearance as continual energy exchange develops between the two- and three-dimensional nonlinear modes, whose large-scale response seems governed by inviscid dynamics but subject to important, continual 'rejuvenation' from small- (fast-) scale viscous action in-between. The three-dimensional growth rate is thereby increased, but not the two-dimensional. Subsequently the disturbed flow enters a higher-amplitude regime similar to that studied in some related papers by the authors and co-workers. Comparisons with the experiments are very supportive of the theory (in the small and in the large), yielding both qualitative and quantitative agreement.

1. Introduction

Our concern in this paper and in some related studies mentioned below is with various types of boundary-layer transition to turbulence, of which there would seem to be quite a number depending on how the transition is initiated. The current study is on resonant-triad interactions in particular.

The possibility of the resonant-triad interaction or nonlinear instability in boundary layers was put forward theoretically by Craik (1971) (see also Raetz 1959; Volodin & Zelman 1978), who proposed that a two-dimensional Tollmien–Schlichting (TS) wave could interact nonlinearly with two oblique three-dimensional TS waves, in such a way that the nonlinear interplay reinforces all three waves. Significantly, this was envisaged as occurring at the (amplitude)^2 order, i.e. 'sooner' than the (amplitude)^3 order of more traditional nonlinear theory. Craik (1971) and later Usher & Craik (1975) and Craik (1978, 1985) gave some supporting analysis, based on guesses or approximations for the interaction coefficients, to illustrate the kind of interplay that might take place. Very recently, careful experimental measurements by Kachanov & Levchenko (1982, 1984), Saric, Kozlov & Levchenko (1984), Saric

† Work performed at: United Technologies Research Center, East Hartford, CT 06108, USA.

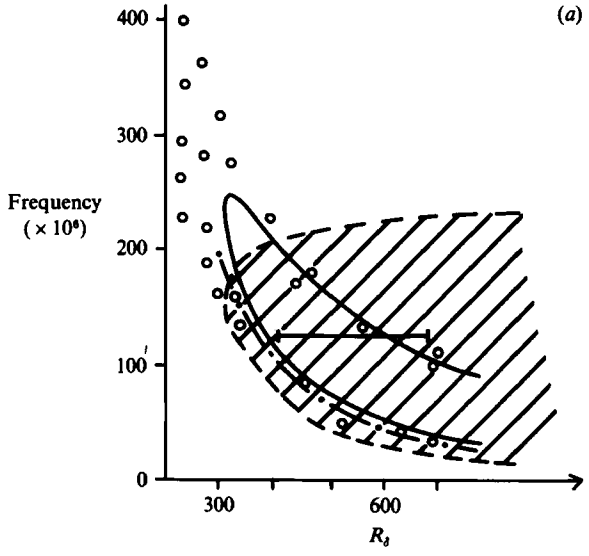
(a)
400
300
200
100
0
Frequency
(× 10⁶)
300
600
R_δ

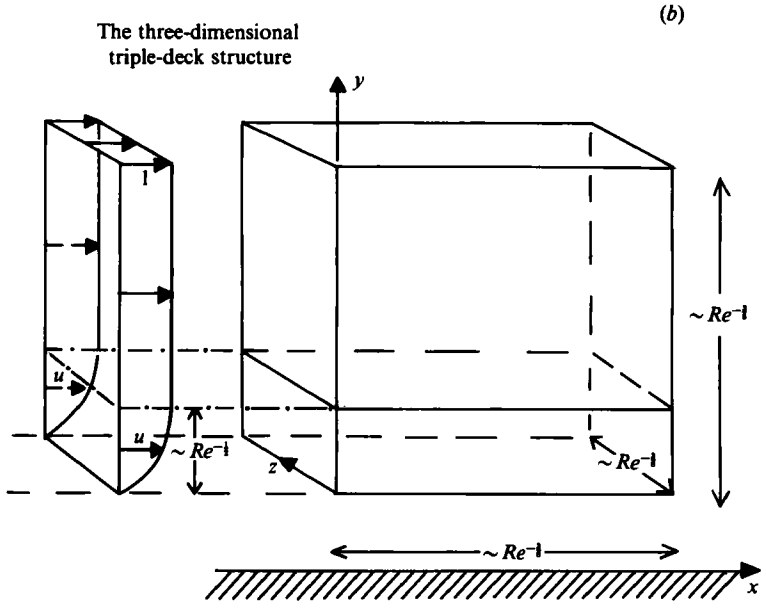
(b)
The three-dimensional
triple-deck structure
y
1
u
u
~ Re⁻¼
z
~ Re⁻¼
~ Re⁻¼
~ Re⁻¼
x

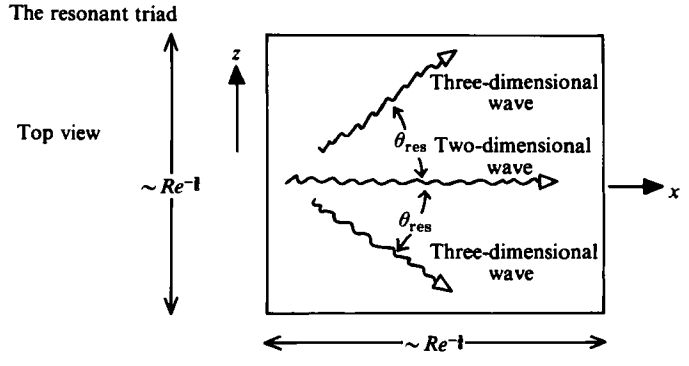
The resonant triad
Top view
z
~ Re⁻¼
Three-dimensional
wave
θres Two-dimensional
wave
θres
Three-dimensional
wave
x
~ Re⁻¼

& Thomas (1984) and references therein, essentially in boundary layers on flat plates, have tended to add considerable weight to Craik's fascinating suggestion, with typical triad formations and the associated growth of subharmonics being observed in unstable boundary layers just prior to transition. Professor M. Gaster (private communication, 1985) also reports significant effects of the (amplitude)^2 sort arising in experimental studies.

The aim in the present work is among other things to investigate on a more rational footing the possibility of such resonant-triad interactions arising in an incompressible boundary layer at high Reynolds number Re, and then to examine the triad properties theoretically and compare these with experiments. Like Smith & Burggraf (1985) and Smith (1986*a*, *b*), who give the background and scalings involved, we choose to address first the local nonlinear unsteady triple-deck problem since it describes the first nonlinear growth of TS disturbances. The scaled governing equations in three dimensions are therefore

$$\frac{\partial U}{\partial X}+\frac{\partial V}{\partial Y}+\frac{\partial W}{\partial Z}=0, \tag{1.1a}$$

$$\frac{\partial U}{\partial T}+\frac{U\partial U}{\partial X}+\frac{V\partial U}{\partial Y}+\frac{W\partial U}{\partial Z}=-\frac{\partial P}{\partial X}(X,Z,T)+\frac{\partial^2 U}{\partial Y^2}, \tag{1.1b}$$

$$\frac{\partial W}{\partial T}+\frac{U\partial W}{\partial X}+\frac{V\partial W}{\partial Y}+\frac{W\partial W}{\partial Z}=-\frac{\partial P}{\partial Z}(X,Z,T)+\frac{\partial^2 W}{\partial Y^2}, \tag{1.1c}$$

and the appropriate boundary conditions include

$$U=V=W=0 \quad \text{at } Y=0, \tag{1.1d}$$

$$U\sim Y+A(X,Z,T), \quad W\to 0, \quad \text{as } Y\to\infty, \tag{1.1e}$$

$$P(X,Z,T)=-\frac{1}{2\pi}\int_{-\infty}^{\infty}\int_{-\infty}^{\infty}\frac{\partial^2 A(\xi,\eta,T)/\partial\xi^2\,\mathrm{d}\xi\,\mathrm{d}\eta}{[(X-\xi)^2+(Z-\eta)^2]^{\frac{1}{2}}}. \tag{1.1f}$$

Here the three-dimensional boundary-layer equations (1.1*a*–*c*) apply in the lower deck, close to the plate surface, where the no-slip condition (1.1*d*) and the displacement condition (1.1*e*) hold, whereas the pressure-displacement law (1.1*f*) stems from the potential-flow properties in the upper deck outside the original $O(Re^{-\frac{1}{8}})$ boundary layer. Also, both the pressure P and the displacement decrement A are unknown functions of X, Z, T, and the domain of interest is $-\infty < X < \infty$, $0 \leqslant Y < \infty$, $-\infty < Z < \infty$, owing to the length scalings noted by Smith & Burggraf (1985) and Smith (1986*a*, *b*). We consider then, typically, the unsteady nonlinear effects produced downstream by a fixed-frequency forcing, or range of frequencies, present upstream.

As an aside, we remark here that the same (relatively high-frequency) flow properties emerge from the scaled system (1.1) as from addressing the Navier–Stokes equations instead with typical non-dimensional pressure levels of order $Re^{-\frac{1}{4}}$ and

---

FIGURE 1. (*a*) A comparison of the typical range (shown shaded) of frequencies and positions x (or Reynolds numbers R_δ based on $x^{\frac{1}{2}}$) covered by multi-structured nonlinear theory, with the typical range (|——|) of the nonlinear-disturbance experiments by Kachanov & Levchenko (1984) [see also Saric *et al.* (1984) and figure 7 below]. Also shown are earlier linear-disturbance properties, for comparison: ○, 'linear' experiments; —·—, linear triple-deck theory from Smith (1979); ——, Orr–Sommerfeld linear calculations, read from Kachanov & Levchenko (1984). (*b*) Schematic diagram of the three-dimensional triple-deck structure for the nonlinear two- and three-dimensional waves forming the resonant triad, with $\theta_{\text{res}} = 60°$, in an originally two-dimensional boundary layer.

non-dimensional time variations between $O(Re^{-\frac{1}{4}})$ and $O(Re^{-\frac{1}{2}})$. The system (1.1), however, is a convenient and in some ways essential starting point: see also comments at the start of §2 below and figure 1. Another aside concerns the practical relevance of asymptotic approaches of the kind used here but this aspect is largely covered already in other studies, by Smith (1979), Smith, Papageorgiou & Elliott (1984), Goldstein (1985), Pedley & Stephanoff (1985) and the present work, for instance, which demonstrate the usefulness of asymptotics in reality, i.e. in numerical terms at finite Reynolds numbers.

In §2 the system (1.1) is analysed for nonlinear disturbances of relatively high frequencies and finite amplitudes. Here we should stress again the point made in some of the references above, that the relatively high frequencies $\Omega \approx |\partial/\partial T|$ correspond either to increased downstream movement of the whole triple-deck interaction, or alternatively to enhanced frequencies input upstream; both of these alternative interpretations are physically meaningful. Provided the large scaled frequency Ω remains less than $O(Re^{\frac{1}{4}})$ the triple-deck structure remains essentially intact, as described in the references mentioned above. For an incoming two-dimensional TS wave, the resonant triad then provokes two subharmonic three-dimensional waves travelling at an angle

$$\theta_{\text{res}} = 60^\circ \tag{1.2}$$

to the free stream, as indeed Craik (1971) notes. The coupled nonlinear evolution equations of the triad are derived in §2. We observe here, in passing, that a resonant triad cannot be set up closer to the lower-branch neutral position further upstream, at finite values of Ω, because of the dispersion relation

$$\mathrm{Ai}'(\xi_0) = \mathrm{e}^{\mathrm{i}\pi/6}\,(\hat{\alpha}^2+\hat{\beta}^2)^{\frac{1}{2}}\hat{\alpha}^{\frac{1}{3}}\int_{\xi_0}^{\infty}\mathrm{Ai}(q)\,\mathrm{d}q \tag{1.3}$$

for small-amplitude waves proportional to $\exp(\mathrm{i}\hat{\alpha}X+\mathrm{i}\hat{\beta}Z-\mathrm{i}\Omega T)$, with $O(1)$ streamwise and spanwise wavenumbers $\hat{\alpha}$, $\hat{\beta}$, and effective frequency Ω, where $\xi_0 \equiv \Omega\exp(-5\mathrm{i}\pi/6)\,\hat{\alpha}^{-\frac{2}{3}}$ and Ai stands for the Airy function. Section 3 presents computational solutions for the central case of temporal triad growth, similar in fact to streamwise spatial growth for which solutions are presented in §5. The growth of all three waves becomes remarkably 'spiky' as time increases, and a large-time/far-downstream analysis (§4) describes the continual exchange of energy and the viscous–inviscid nature of the spikes produced. Further discussion, and a spatial solution, are given in §5.

Overall, the present study fully supports Craik's (1971) original suggestion, and puts it on a more rational foundation, we believe. The interaction coefficients, however, found in §2, are such that the finite-time or -distance breakdown also postulated by Craik cannot occur, at least in the present regime. Instead, the eventual growth rate is the same as in linear two-dimensional theory, as §4 and the Appendix show. Thus, although the nonlinear–triad interplay does occur 'soon', at quite low amplitudes, and then does enhance the growth of the three-dimensional components of the disturbance, the eventual outcome of the interaction is that the developing disturbance appears to move on, next, into a higher-amplitude regime which is much (although not entirely) as in the two-dimensional case of Smith (1986*a*), and this is addressed in a companion study (Smith 1986*b*). This later regime produces significantly stronger growth.

Alternative nonlinear three-dimensional interactions, and comparisons with the recent experiments on slower transition, are also discussed in §5. The experimental

comparisons seem very encouraging (on the small- and the large-scale behaviour), yielding both qualitative and quantitative agreement.

2. The resonant–triad interaction

The nonlinear system (1.1) is studied here for finite amplitudes of pressure $|P|$ and high frequencies $\Omega[\approx |\partial/\partial T|]$, for two main reasons. First, the experiments referred to in §1 tend to indicate that the possible formation of triads is quite far downstream of the lower-branch neutral curve (see figures 1–4 of Saric *et al.* (1984), and our figure 1), which corresponds to increased Ω in our scalings. Secondly, high-frequency properties can shed much light analytically (Smith & Burggraf 1985; Smith 1986*a*, *b*) on the whole ensuing transition process, we feel, as opposed perhaps to the full system (1.1) which in general requires quite large-scale computational efforts, although again the full system (1.1) undoubtedly represents a most significant step in transition.

After some preliminary order-of-magnitude estimates, the multiple scales

$$\frac{\partial}{\partial T} \rightarrow \Omega \frac{\partial}{\partial T_0} + \frac{\partial}{\partial T_2} + \ldots, \tag{2.1a}$$

$$\frac{\partial}{\partial X} \rightarrow \Omega^{\frac{1}{2}} \frac{\partial}{\partial X_0} + \Omega^{-\frac{1}{2}} \frac{\partial}{\partial X_2} + \ldots, \tag{2.1b}$$

$$\frac{\partial}{\partial Z} \rightarrow \Omega^{\frac{1}{2}} \frac{\partial}{\partial Z_0} + \Omega^{-\frac{1}{2}} \frac{\partial}{\partial Z_2} + \ldots \tag{2.1c}$$

are implied, cf. the three references just above and §5. Here

$$(X, Z) = \Omega^{-\frac{1}{2}}(X_0, Z_0) = \Omega^{\frac{1}{2}}(X_2, Z_2), \quad T = \Omega^{-1} T_0 = T_2,$$

and so on, and the expansions below proceed in inverse powers of Ω. Bearing in mind the general eigenrelation in (1.3) for linear three-dimensional waves, and in particular its high-frequency form

$$\hat{\alpha}^2(\hat{\alpha}^2 + \hat{\beta}^2) = \Omega^2 \tag{2.2}$$

at leading order, we take $(\hat{\alpha}, \hat{\beta}) = \Omega^{\frac{1}{2}}(\alpha, \beta)$ to leading order and consider three nonlinear waves proportional to

$$E_1 \equiv \exp[\mathrm{i}\alpha X_0 - \mathrm{i} T_0] \quad \text{(two-dimensional)}, \tag{2.3a}$$

$$E_2, E_3 \equiv \exp[\tfrac{1}{2}\mathrm{i}\alpha X_0 \pm \mathrm{i}\beta Z_0 - \tfrac{1}{2}\mathrm{i} T_0] \quad \text{(three-dimensional)}. \tag{2.3b, c}$$

These form a resonant triad at (amplitude)^2 order since, for example, the nonlinear combination $E_2 E_3$ reproduces the two-dimensional wave E_1:

$$E_2 E_3 = E_1. \tag{2.3d}$$

For the two-dimensional wave (2.3*a*) and the subharmonics (2.3*b*, *c*) to be able to start as TS waves, however, (2.2) then requires that

$$\alpha = 1, \quad \beta = \frac{\sqrt{3}}{2}, \tag{2.4}$$

because to leading order we have, in (2.2), $(\hat{\alpha}, \hat{\beta}, \Omega) \rightarrow (\frac{1}{2}\alpha\Omega^{\frac{1}{2}}, \pm\beta\Omega^{\frac{1}{2}}, \frac{1}{2}\Omega)$ for E_2, E_3 and $(\hat{\alpha}, \hat{\beta}, \Omega) \rightarrow (\alpha\Omega^{\frac{1}{2}}, 0, \Omega)$ for E_1. So, from (2.4), the three-dimensional waves in (2.3*b*, *c*) are inclined at an angle to the free-stream direction of

$$\theta_{\mathrm{res}} = 60°, \tag{2.5}$$

as Craik (1971) notes. The accompanying pressure and negative displacement expansions are

$$P = P_0 + \Omega^{-1} P_2 + \ldots, \tag{2.6a}$$

$$A = \Omega^{-\frac{1}{2}} A_0 + \Omega^{-\frac{3}{2}} A_2 + \ldots, \tag{2.6b}$$

where P_0, A_0 contain the three waves of (2.3),

$$(P_0, A_0) = (P_{01}, A_{01})\, E_1 + (P_{02}, A_{02})\, E_2 + (P_{03}, A_{03})\, E_3 + \text{c.c.}, \tag{2.7}$$

while P_2, A_2 are produced by nonlinear interactions and so have the forms

$$(P_2, A_2) = (P_{21}, A_{21})\, E_1 + (P_{22}, A_{22})\, E_2 + (P_{23}, A_{23})\, E_3 + \text{c.c.} + [\text{other products of } E_1^{\pm 1}, E_2^{\pm 1}, E_3^{\pm 1}] \tag{2.8}$$

in view of (3.2*d*). Here c.c. denotes the complex conjugate. We observe that the main pressure P in (2.6*a*) and the corresponding disturbance amplitudes below are much less, for this triad interaction, than in the nonlinear response studied by Smith & Burggraf (1985) and Smith (1986*a*) for two-dimensional flows and Smith (1986*b*) for three-dimensional properties; this indeed is the potential power of the three-dimensional triad interaction. Another observation here is that a mean-flow correction arises among the other terms in (2.8) but this correction, although awkward to evaluate, does not influence the triad interaction below to any significant extent.

Two regions I, II in the Y-direction then need to be investigated.

2.1. *The Stokes layer I*

In the thin viscous Stokes layer I, $y = \Omega^{-\frac{1}{2}} \tilde{y}$ with $\tilde{y}$ of $O(1)$, and the velocity field has the form

$$(U, V, W) = \Omega^{-\frac{1}{2}} (U_0, V_0, W_0) + \Omega^{-\frac{3}{2}} (U_2, V_2, W_2) + \ldots. \tag{2.9}$$

As mentioned before, the disturbance amplitude here does not need to be as large as in the amplitude-cubed-interaction cases of the three last-named papers for nonlinear effects to matter. In fact the disturbance is comparable in size with the original basic flow, with

$$U_0 = (U_{01} E_1 + U_{02} E_2 + U_{03} E_3) + \text{c.c.} + U_{0M}, \tag{2.10}$$

and similarly for V_0, W_0; here $U_{0M} \equiv \tilde{y}$ gives the important basic motion, from (1.1), and $V_{0M} = W_{0M} \equiv 0$. Also, since E_1 is the incoming two-dimensional wave, $W_{01} \equiv 0$.

The governing equations for the dominant velocities in layer I form an unsteady pressure gradient–viscous force balance throughout,

$$-\mathrm{i} U_{01} = -\mathrm{i} P_{01} + \frac{\partial^2 U_{01}}{\partial \tilde{y}^2}, \tag{2.11a}$$

$$-\tfrac{1}{2}\mathrm{i}\, U_{02} = -\tfrac{1}{2}\mathrm{i}\, P_{02} + \frac{\partial^2 U_{02}}{\partial \tilde{y}^2}, \quad -\tfrac{1}{2}\mathrm{i}\, W_{02} = -\mathrm{i}\beta P_{02} + \frac{\partial^2 W_{02}}{\partial \tilde{y}^2}, \tag{2.11b,c}$$

$$-\tfrac{1}{2}\mathrm{i}\, U_{03} = -\tfrac{1}{2}\mathrm{i}\, P_{03} + \frac{\partial^2 U_{03}}{\partial \tilde{y}^2}, \quad -\tfrac{1}{2}\mathrm{i}\, W_{03} = +\mathrm{i}\beta P_{03} + \frac{\partial^2 W_{03}}{\partial \tilde{y}^2}, \tag{2.11d,e}$$

along with the continuity equations

$$\mathrm{i} U_{01} + \frac{\partial V_{01}}{\partial \tilde{y}} = 0, \quad \tfrac{1}{2}\mathrm{i}\, U_{02,3} + \frac{\partial V_{02,3}}{\partial \tilde{y}} \pm \mathrm{i}\beta W_{02,3} = 0 \tag{2.11f–h}$$

from (1.1). The solutions satisfying the no-slip conditions at $\tilde{y} = 0$ and appropriate boundedness as $\tilde{y} \to \infty$ are therefore

$$U_{01} = P_{01}(1-\mathrm{e}^{m\tilde{y}}), \quad U_{02,3} = P_{02,3}(1-\mathrm{e}^{\tilde{m}\tilde{y}}), \tag{2.12}$$

$$W_{02,3} = \pm 2\beta P_{02,3}(1-\mathrm{e}^{\tilde{m}\tilde{y}}), \tag{2.13}$$

$$V_{01} = -\mathrm{i}P_{01}\left(\tilde{y}-\frac{\mathrm{e}^{m\tilde{y}}}{m}+\frac{1}{m}\right), \quad V_{02,3} = -2\mathrm{i}(\tfrac{1}{4}+\beta^2)\,P_{02,3}\left(\tilde{y}-\frac{\mathrm{e}^{\tilde{m}\tilde{y}}}{\tilde{m}}+\frac{1}{\tilde{m}}\right), \tag{2.14}$$

where $m = \exp(3\pi\mathrm{i}/4)\,[= \tilde{m}\sqrt{2}]$.

At the next order, the governing equations for (U_2, V_2, W_2) pick up nonlinear inertial effects involving (U_0, V_0, W_0) from (1.1). If

$$U_2 = (U_{21}E_1 + U_{22}E_2 + U_{23}E_3) + \text{c.c.} + [\text{other nonlinear terms}] \tag{2.15}$$

and similarly for V_2, W_2, then, with (U_0, V_0, W_0) given in (2.10)–(2.14), the following successive equations hold:

Continuity:

$$\mathrm{i}U_{21} + \frac{\partial U_{01}}{\partial X_2} + \frac{\partial V_{21}}{\partial \tilde{y}} = 0, \tag{2.16a}$$

$$\tfrac{1}{2}\mathrm{i}U_{2n} + \frac{\partial U_{0n}}{\partial X_2} + \frac{\partial V_{2n}}{\partial \tilde{y}} \pm \mathrm{i}\beta W_{2n} + \frac{\partial W_{0n}}{\partial Z_2} = 0; \tag{2.16b}$$

X-momentum:

$$-\mathrm{i}U_{21} + (1-\mathrm{e}^{m\tilde{y}})\frac{\partial P_{01}}{\partial T_2} + \mathrm{i}P_{02}P_{03}(1-\mathrm{e}^{\tilde{m}\tilde{y}})^2(1-4\beta^2)$$

$$+\mathrm{i}\tilde{m}P_{02}P_{03}\,\mathrm{e}^{\tilde{m}\tilde{y}}\left(\tilde{y}-\frac{\mathrm{e}^{\tilde{m}\tilde{y}}}{\tilde{m}}+\frac{1}{\tilde{m}}\right)(\tfrac{1}{4}+\beta^2) + \mathrm{i}P_{01}\left(-\tilde{y}\,\mathrm{e}^{m\tilde{y}} + \frac{\mathrm{e}^{m\tilde{y}}}{m} - \frac{1}{m}\right)$$

$$= -\mathrm{i}P_{21} - \frac{\partial P_{01}}{\partial X_2} + \frac{\partial^2 U_{21}}{\partial \tilde{y}^2}, \tag{2.17a}$$

$$-\tfrac{1}{2}\mathrm{i}U_{2n} + (1-\mathrm{e}^{\tilde{m}\tilde{y}})\frac{\partial P_{0n}}{\partial T_2} + \tfrac{1}{2}\mathrm{i}P_{01}P^*_{03,2}(1-\mathrm{e}^{m\tilde{y}})(1-\mathrm{e}^{\tilde{m}^*\tilde{y}})$$

$$+\mathrm{i}\tilde{m}^*P_{01}P^*_{03,2}\,\mathrm{e}^{\tilde{m}^*\tilde{y}}\left(\tilde{y}-\frac{\mathrm{e}^{m\tilde{y}}}{m}+\frac{1}{m}\right) - 2\mathrm{i}mP_{01}P^*_{03,2}\,\mathrm{e}^{m\tilde{y}}\left(\tilde{y}-\frac{\mathrm{e}^{\tilde{m}^*\tilde{y}}}{\tilde{m}^*}+\frac{1}{\tilde{m}^*}\right)(\tfrac{1}{4}+\beta^2)$$

$$+\tfrac{1}{2}\mathrm{i}\tilde{y}P_{0n}(1-\mathrm{e}^{\tilde{m}\tilde{y}}) - 2\mathrm{i}(\tfrac{1}{4}+\beta^2)\,P_{0n}\left(\tilde{y}-\frac{\mathrm{e}^{\tilde{m}\tilde{y}}}{\tilde{m}}+\frac{1}{\tilde{m}}\right) = -\tfrac{1}{2}\mathrm{i}P_{2n} - \frac{\partial P_{0n}}{\partial X_2} + \frac{\partial^2 U_{2n}}{\partial \tilde{y}^2}; \tag{2.17b}$$

Z-momentum:

$$-\mathrm{i}W_{21} = -\frac{\partial P_{01}}{\partial Z_2} + \frac{\partial^2 W_{21}}{\partial \tilde{y}^2}, \tag{2.18a}$$

$$-\tfrac{1}{2}\mathrm{i}W_{2n} + 2\beta(1-\mathrm{e}^{\tilde{m}\tilde{y}})\frac{\partial P_{0n}}{\partial T_2} + \mathrm{i}\beta P_{01}P^*_{03,2}(1-\mathrm{e}^{m\tilde{y}})(1-\mathrm{e}^{\tilde{m}^*\tilde{y}})$$

$$-2\mathrm{i}\beta\tilde{m}^*P_{01}P^*_{03,2}\,\mathrm{e}^{\tilde{m}^*\tilde{y}}\left(\tilde{y}-\frac{\mathrm{e}^{m\tilde{y}}}{m}+\frac{1}{m}\right) + \mathrm{i}\tilde{y}\beta P_{0n}(1-\mathrm{e}^{\tilde{m}\tilde{y}})$$

$$= -\mathrm{i}\beta P_{2n} - \frac{\partial P_{0n}}{\partial Z_2} + \frac{\partial^2 W_{2n}}{\partial \tilde{y}^2}, \tag{2.18b}$$

for $n = 2, 3$, where (2.3d) has been used and * denotes the complex conjugate. As far

as the subsequent working is concerned, however, only the large-$\tilde{y}$ forms emerging from (2.17) and (2.18) are needed, and these are

$$U_{21} \to \left[-\mathrm{i}\frac{\partial P_{01}}{\partial T_2} + P_{02}P_{03}(1-4\beta^2) - \frac{P_{01}}{m} + P_{21} - \mathrm{i}\frac{\partial P_{01}}{\partial X_2}\right], \tag{2.19a}$$

$$U_{2n} \sim -4\beta^2 P_{0n}\tilde{y} + \left[-2\mathrm{i}\frac{\partial P_{0n}}{\partial T_2} + P_{01}P^*_{03,2} - (1+4\beta^2)\frac{P_{0n}}{\tilde{m}} + P_{2n} - 2\mathrm{i}\frac{\partial P_{0n}}{\partial X_2}\right], \tag{2.19b}$$

$$W_{21} \to \left[-\mathrm{i}\frac{\partial P_{01}}{\partial Z_2}\right], \tag{2.19c}$$

$$W_{2n} \sim 2\beta P_{0n}\tilde{y} + \left[\mp 4\mathrm{i}\beta\frac{\partial P_{0n}}{\partial T_2} \pm 2\beta P_{01}P^*_{03,2} \pm 2\beta P_{2n} - 2\mathrm{i}\frac{\partial P_{0n}}{\partial Z_2}\right], \tag{2.19d}$$

for $\tilde{y} \to \infty$. The above forms are to be matched to the outer region II discussed next.

2.2. *The outer region II*

This outer region II is mainly inviscid, containing a critical layer, and is required as a non-trivial buffer between the Stokes layer and the outer constraints in (1.1). In region II we have $Y = \Omega^{\frac{1}{2}}\hat{y}$ with $\hat{y}$ now of order unity, and the velocity expansions

$$U = \Omega^{\frac{1}{2}}\hat{y} + \Omega^{-\frac{1}{2}}\hat{U}_0 + \Omega^{-\frac{3}{2}}\hat{U}_2 + \ldots, \quad V = \Omega^{\frac{1}{2}}\hat{V}_0 + \Omega^{-\frac{1}{2}}\hat{V}_2 + \ldots, \tag{2.20a,b}$$

$$W = \Omega^{-\frac{1}{2}}\hat{W}_0 + \Omega^{-\frac{3}{2}}\hat{W}_2 + \ldots. \tag{2.20c}$$

Here the successive components split up into the three waves of (2.3*a–c*) in the manner

$$\hat{U}_0 = (\hat{U}_{01}E_1 + \hat{U}_{02}E_2 + \hat{U}_{03}E_3) + \text{c.c.}, \tag{2.21a}$$

$$\hat{U}_2 = (\hat{U}_{21}E_1 + \hat{U}_{22}E_2 + \hat{U}_{23}E_3) + \text{c.c.} + [\text{other nonlinear terms}], \tag{2.21b}$$

with similar expressions for the $\hat{V}$ and $\hat{W}$. The dominant terms are then controlled, from substitution into (1.1), by the equations

$$\mathrm{i}\hat{U}_{01} + \frac{\partial \hat{V}_{01}}{\partial \hat{y}} = 0, \quad \mathrm{i}(\hat{y}-1)\hat{U}_{01} + \hat{V}_{01} = -\mathrm{i}P_{01}, \tag{2.22a}$$

$$\tfrac{1}{2}\mathrm{i}\hat{U}_{02,3} + \frac{\partial \hat{V}_{02,3}}{\partial \hat{y}} \pm \mathrm{i}\beta\hat{W}_{02,3} = 0, \quad \tfrac{1}{2}\mathrm{i}(\hat{y}-1)\hat{U}_{02,3} + \hat{V}_{02,3} = -\tfrac{1}{2}\mathrm{i}P_{02,3}, \tag{2.22b}$$

$$\tfrac{1}{2}\mathrm{i}(\hat{y}-1)\hat{W}_{02,3} = \mp\mathrm{i}\beta P_{02,3}, \tag{2.22c}$$

representing the dominant unsteady inertial–pressure gradient balances. The critical layer occurs at $\hat{y} = 1$ throughout, but is a passive affair as in Smith & Burggraf (1985) and Smith (1986*a*, *b*).

The solutions of (2.22) satisfying the required outer constraints in (1.1) follow as

$$\hat{U}_{01} = A_{01}, \quad \hat{V}_{01} = -\mathrm{i}A_{01}\hat{y} (\hat{W}_{01} \equiv 0), \tag{2.23a}$$

$$\hat{U}_{02,3} = A_{02,3} + \frac{4\beta^2 P_{02,3}}{(\hat{y}-1)}, \quad \hat{W}_{02,3} = \frac{\mp 2\beta P_{02,3}}{(\hat{y}-1)}, \quad \hat{V}_{02,3} = -\tfrac{1}{2}\mathrm{i}A_{02,3}\hat{y}, \tag{2.23b,c}$$

while the merging with the earlier Stokes-layer solutions as $\hat{y} \to 0+$ yields

$$A_{01} = P_{01}, \quad A_{02,3} = (1+4\beta^2)P_{02,3}, \tag{2.23d}$$

which are the first pressure-displacement relations.

Nonlinear effects again enter the reckoning at the next order, where the controlling equations of concern are the following:

Continuity:

$$\mathrm{i}\hat{U}_{21}+\frac{\partial \hat{U}_{01}}{\partial X_2}+\frac{\partial \hat{V}_{21}}{\partial \hat{y}}=0, \tag{2.24a}$$

$$\tfrac{1}{2}\mathrm{i}\hat{U}_{22,3}+\frac{\partial \hat{U}_{02,3}}{\partial X_2}+\frac{\partial \hat{V}_{22,3}}{\partial \hat{y}}\pm\mathrm{i}\beta\hat{W}_{22,3}+\frac{\partial \hat{W}_{02,3}}{\partial Z_2}=0; \tag{2.24b,c}$$

X-momentum:

$$\mathrm{i}(\hat{y}-1)\,\hat{U}_{21}+\frac{\partial \hat{U}_{01}}{\partial T_2}+\hat{y}\,\frac{\partial \hat{U}_{01}}{\partial X_2}+\hat{V}_{21}$$
$$+\left\{\mathrm{i}\hat{U}_{02}\,\hat{U}_{03}+\hat{V}_{02}\,\frac{\partial \hat{U}_{03}}{\partial \hat{y}}+\hat{V}_{03}\,\frac{\partial \hat{U}_{02}}{\partial \hat{y}}-\mathrm{i}\beta\hat{W}_{02}\,\hat{U}_{03}+\mathrm{i}\beta\hat{W}_{03}\,\hat{U}_{02}\right\}=-\mathrm{i}P_{21}-\frac{\partial P_{01}}{\partial X_2}, \tag{2.25a}$$

$$\tfrac{1}{2}\mathrm{i}(\hat{y}-1)\,\hat{U}_{22,3}+\frac{\partial \hat{U}_{02,3}}{\partial T_2}+\hat{y}\,\frac{\partial \hat{U}_{02,3}}{\partial X_2}+\hat{V}_{22,3}$$
$$+\left\{\tfrac{1}{2}\mathrm{i}\hat{U}^{*}_{03,2}\,\hat{U}_{01}+\hat{V}_{01}\,\frac{\partial \hat{U}^{*}_{03,2}}{\partial \hat{y}}\right\}=-\tfrac{1}{2}\mathrm{i}P_{22,3}-\frac{\partial P_{02,3}}{\partial X_2}; \tag{2.25b,c}$$

Z-momentum:

$$\mathrm{i}(\hat{y}-1)\,\hat{W}_{21}+\left\{\tfrac{1}{2}\mathrm{i}\hat{U}_{02}\,\hat{W}_{03}+\tfrac{1}{2}\mathrm{i}\hat{U}_{03}\,\hat{W}_{02}+\hat{V}_{02}\,\frac{\partial \hat{W}_{03}}{\partial \hat{y}}+\hat{V}_{03}\,\frac{\partial \hat{W}_{02}}{\partial \hat{y}}\right\}=-\frac{\partial P_{01}}{\partial Z_2}, \tag{2.26a}$$

$$\tfrac{1}{2}\mathrm{i}(\hat{y}-1)\,\hat{W}_{22,3}+\frac{\partial \hat{W}_{02,3}}{\partial T_2}+\hat{y}\,\frac{\partial \hat{W}_{02,3}}{\partial X_2}$$
$$+\left\{-\tfrac{1}{2}\mathrm{i}\hat{U}_{01}\,\hat{W}^{*}_{03,2}+\hat{V}_{01}\,\frac{\partial \hat{W}^{*}_{03,2}}{\partial \hat{y}}\right\}=\mp\mathrm{i}\beta P_{22,3}-\frac{\partial P_{02,3}}{\partial Z_2}. \tag{2.26b,c}$$

Here the nonlinearly induced effects are shown in curly brackets. Also, the join with the outer constraints of (1.1) and with the Stokes layer, respectively, requires that

$$\hat{U}_{2n}\to A_{2n},\quad \hat{W}_{2n}\to 0,\quad \text{as } \hat{y}\to\infty, \tag{2.27a}$$

$$\left.\begin{aligned}\hat{U}_{2n}&\to U_{2n\infty},\quad \hat{W}_{2n}\to W_{2n\infty}\\ \hat{V}_{21}&\to\frac{-\mathrm{i}P_{01}}{m},\quad \hat{V}_{22,3}\to-2\mathrm{i}(\tfrac{1}{4}+\beta^2)\,\frac{P_{02,3}}{m}\end{aligned}\right\}\ \text{as } \hat{y}\to 0+, \tag{2.27b}$$

for $n=1,2,3$, where $U_{2n\infty}$, $W_{2n\infty}$ stand for the $O(1)$ contributions shown in square brackets in (2.19). The conditions on $\hat{U}_{2n}$, $\hat{W}_{2n}$ are applied below. The rest of the matching then goes through satisfactorily, including the non-zero contributions to the $\hat{V}$ in (2.27*b*), bringing in the viscous-sublayer displacements, from (2.14), which are ultimately responsible for the growth terms in the amplitude equations of §2.3 below.

The flow solutions satisfying the outer constraints (2.27*a*) are therefore of the form

$$\hat{U}_{21}=A_{21}+\hat{C}_{21}(\hat{y}-1)^{-2}+\hat{D}_{21}(\hat{y}-1)^{-3}, \tag{2.28a}$$

with

$$\left.\begin{aligned}\hat{C}_{21}&\equiv-8\beta^2(1+4\beta^2)\,P_{02}\,P_{03},\\ \hat{D}_{21}&\equiv-\tfrac{8}{3}\beta^2(1+12\beta^2)\,P_{02}\,P_{03}\end{aligned}\right\} \tag{2.28b}$$

and, for $n = 2, 3$ in turn,

$$\hat{U}_{2n} \pm 2\beta \hat{W}_{2n} = A_{2n} + \hat{B}_{2n}(\hat{y}-1)^{-1} + \hat{C}_{2n}(\hat{y}-1)^{-2} + \hat{D}_{2n}(\hat{y}-1)^{-3}, \tag{2.28c}$$

with

$$\left.\begin{aligned} \hat{B}_{2n} &\equiv 4\mathrm{i}\beta\left(2\beta \frac{\partial P_{0n}}{\partial X_2} \mp \frac{\partial P_{0n}}{\partial Z_2}\right), \\ \hat{C}_{2n} &\equiv -8\beta^2 P_{01} P^*_{03,\,2}, \quad \hat{D}_{2n} \equiv -\tfrac{32}{3}\beta^2 P_{01} P^*_{03,\,2}. \end{aligned}\right\} \tag{2.28d}$$

The inner constraints (2.27*b*) then require

$$\left.\begin{aligned} A_{21} + \hat{C}_{21} - \hat{D}_{21} &= U_{21\infty}, \\ A_{2n} - \hat{B}_{2n} + \hat{C}_{2n} - \hat{D}_{2n} &= U_{2n\infty} \pm 2\beta W_{2n\infty} \quad (n = 2, 3), \end{aligned}\right\} \tag{2.29}$$

which constitute the second pressure–displacement relations.

2.3. *The pressure-displacement interaction, and the triad-amplitude equations*

The pressure-displacement interaction law in (1.1*f*) now provides the relations, complementary to (2.23*d*), (2.29), to determine the triad equations. From (1.1*f*), with the substitutions (2.1), (2.6), we find, first, exactly the relations (2.23*d*) again, thus verifying the values of α, β in (2.4). Secondly, we have the relations

$$-P_{21} + \frac{\mathrm{i}\,\partial P_{01}}{\partial X_2} = -A_{21} + 2\mathrm{i}\frac{\partial A_{01}}{\partial X_2}, \tag{2.30a}$$

$$-(\tfrac{1}{4}+\beta^2)^{\frac{1}{2}} P_{2n} + \mathrm{i}(\tfrac{1}{4}+\beta^2)^{-\frac{1}{2}}\left(\frac{1}{2}\frac{\partial P_{0n}}{\partial X_2} \pm \beta \frac{\partial P_{0n}}{\partial Z_2}\right) = -\tfrac{1}{4}A_{2n} + \mathrm{i}\frac{\partial A_{0n}}{\partial X_2} \tag{2.30b}$$

for $n = 2, 3$ respectively.

When (2.30*a*, *b*) are coupled with (2.29) and the definitions in (2.28*b*, *d*), the P_{2n} and A_{2n} contributions cancel out for $n = 1, 2, 3$, as expected, leaving the nonlinear amplitude equations

$$\frac{\partial P_{01}}{\partial T_2} + 2\frac{\partial P_{01}}{\partial X_2} = \left(\frac{1-\mathrm{i}}{\sqrt{2}}\right) P_{01} - 2\mathrm{i} P_{02} P_{03}, \tag{2.31a}$$

$$\frac{\partial P_{02}}{\partial T_2} + \frac{5}{4}\frac{\partial P_{02}}{\partial X_2} + \frac{\sqrt{3}}{4}\frac{\partial P_{02}}{\partial Z_2} = \left(\frac{1-\mathrm{i}}{2}\right) P_{02} - \tfrac{1}{4}\mathrm{i} P_{01} P^*_{03}, \tag{2.31b}$$

$$\frac{\partial P_{03}}{\partial T_2} + \frac{5}{4}\frac{\partial P_{03}}{\partial X_2} - \frac{\sqrt{3}}{4}\frac{\partial P_{03}}{\partial Z_2} = \left(\frac{1-\mathrm{i}}{2}\right) P_{03} - \tfrac{1}{4}\mathrm{i} P_{01} P^*_{02}, \tag{2.31c}$$

of the resonant triad for P_{01}, P_{02}, P_{03}, after some manipulation. Here the linear terms contained in (2.31) all agree with, and could be derived directly from, a higher-order version of (2.2) in which the term Ω^2, on the right-hand side of (2.2), is multiplied by $[1 + 2\alpha\Omega^{-\frac{3}{2}} \exp(5\pi\mathrm{i}/4) + O(\alpha^2\Omega^{-3})]$ to incorporate the relatively slow growth present. The linear terms above also show the group velocities of the individual waves (2.3*a–c*) appearing, via the left-hand sides in (2.31), while the linear growth terms proportional to $(1-\mathrm{i})$ on the right-hand sides are due to viscous effects. The nonlinear (amplitude)^2 terms, in contrast, stemming mainly from region II, seem to require the fuller derivation given in §§2.1, 2.2, which also helps to emphasize the rich structure of the present flow regime. These nonlinear terms (in (2.31)) have one essential difference from the forms suggested in Craik (1971). It is that their coefficients are all purely imaginary and equisigned. This tends to rule out a number of the nonlinear responses conjectured by Craik, including the possibility of a finite-time or -space breakdown.

Extensions and other aspects of the amplitude equations (2.31*a–c*) and certain special cases are mentioned in §5 below. For now, however, as a start, attention is

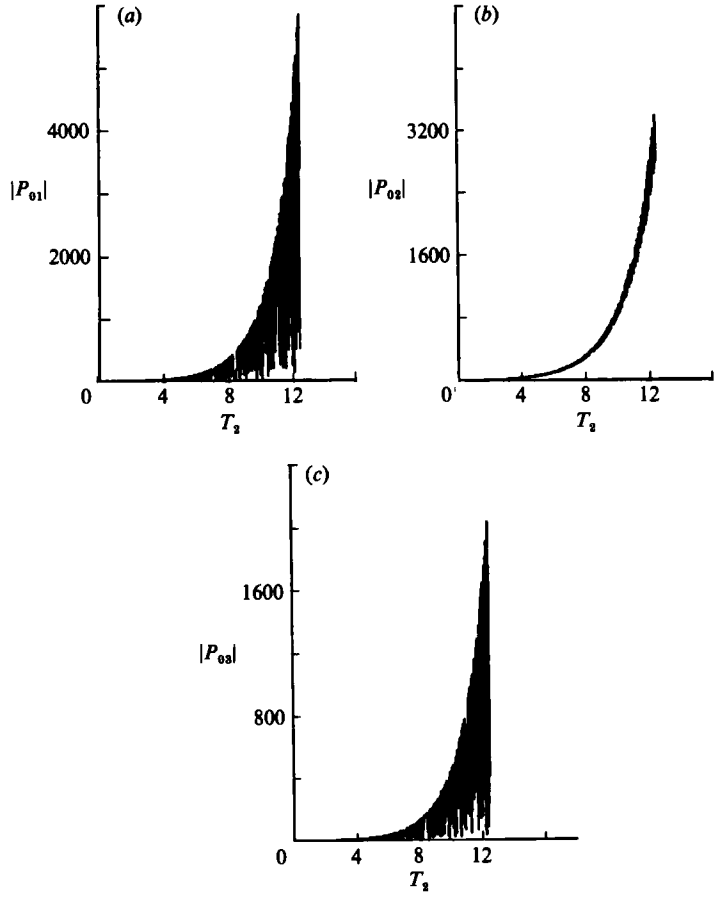

FIGURE 2. Numerical solutions of the temporal resonant-triad equations (3.1*a–c*), with $P_{03} \not\equiv P_{02}$ (see also the spatial case in figure 6). Here $\Delta = 0.00000625$ and the plot interval is 0.0125, i.e. the results at every 2000th time step are plotted. Initial values are $P_{01,\,2,\,3} = 0, 5, 1$, respectively. Shown are (*a*) $|P_{01}|$, (*b*) $|P_{02}|$, (*c*) $|P_{03}|$.

focused on the special case of plane waves where the spatial derivatives in X_2, Z_2 are absent (see further comments on the spatial problem in §5), and (2.31*a–c*) then reduce to a set of coupled nonlinear ordinary differential equations for P_{01}, P_{02}, P_{03}, defining one central class of resonant triads.

3. Numerical method and results

If the X_2 and Z_2 dependence is absent, (2.31*a–c*) reduce to the nonlinear complex ordinary differential system

$$\frac{dP_{01}}{dT_2} = \left(\frac{1-i}{\sqrt{2}}\right) P_{01} - 2iP_{02}P_{03}, \tag{3.1a}$$

$$\frac{dP_{02}}{dT_2} = \left(\frac{1-i}{2}\right) P_{02} - \tfrac{1}{4}iP_{01}P_{03}^*, \tag{3.1b}$$

$$\frac{dP_{03}}{dT_2} = \left(\frac{1-i}{2}\right) P_{03} - \tfrac{1}{4}iP_{01}P_{02}^*, \tag{3.1c}$$

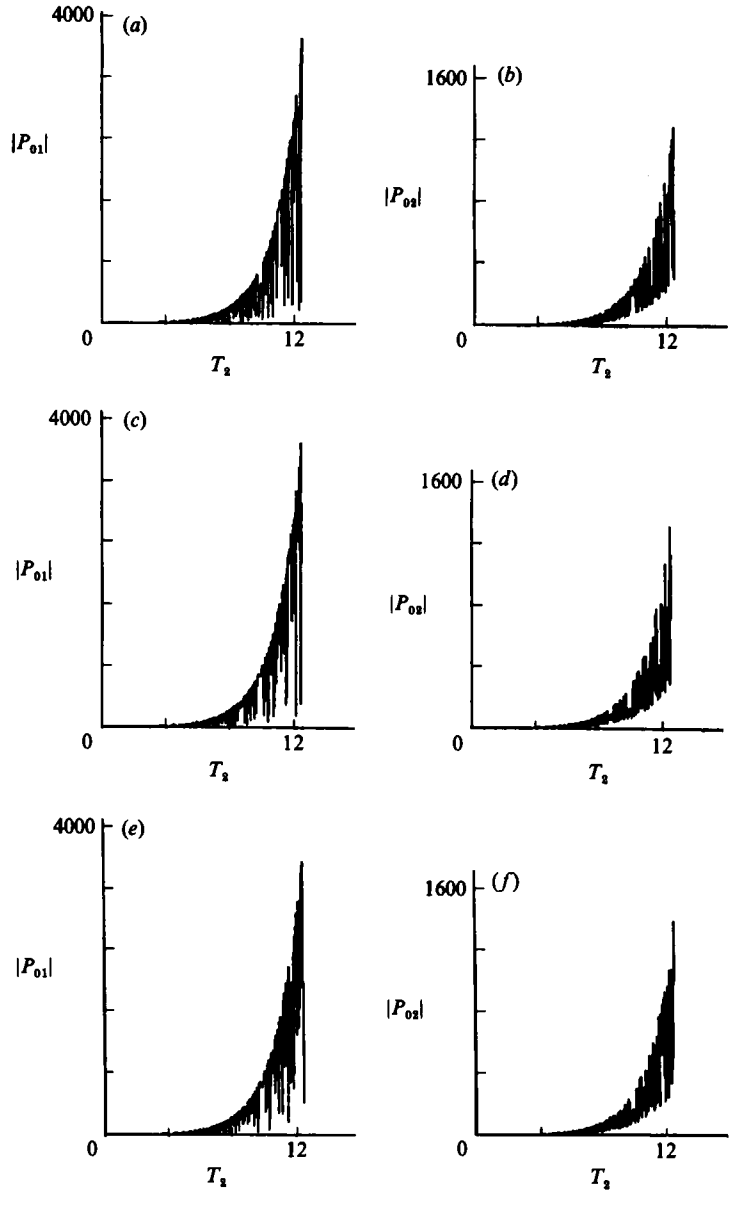

FIGURE 3. Numerical solutions of (3.1), with $P_{03} = P_{02}$, for various time steps Δ (see also the spatial case in figure 6). The plot interval is 0.025 throughout and the initial values are $P_{01,2} = 1+\mathrm{i}, 0.5$. (*a*), (*b*) give $|P_{01}|, |P_{02}|$ respectively for $\Delta = 0.00005$; (*c*), (*d*) as (*a*), (*b*) but $\Delta = 0.000025$; (*e*), (*f*) as (*a*), (*b*) but $\Delta = 0.0000125$.

which we address numerically here. A simple second-order predictor–corrector scheme was used to obtain computational results for various starting conditions at time $T_2 = 0$. For each small time step Δ, the predictor and corrector parts take the form

$$P_{01}\text{-pred} = \overline{P_{01}} + \Delta\left[\frac{(1-\mathrm{i})\,\overline{P_{01}}}{\sqrt{2}} - 2\mathrm{i}\overline{P_{02}}\,\overline{P_{03}}\right] \tag{3.2a}$$

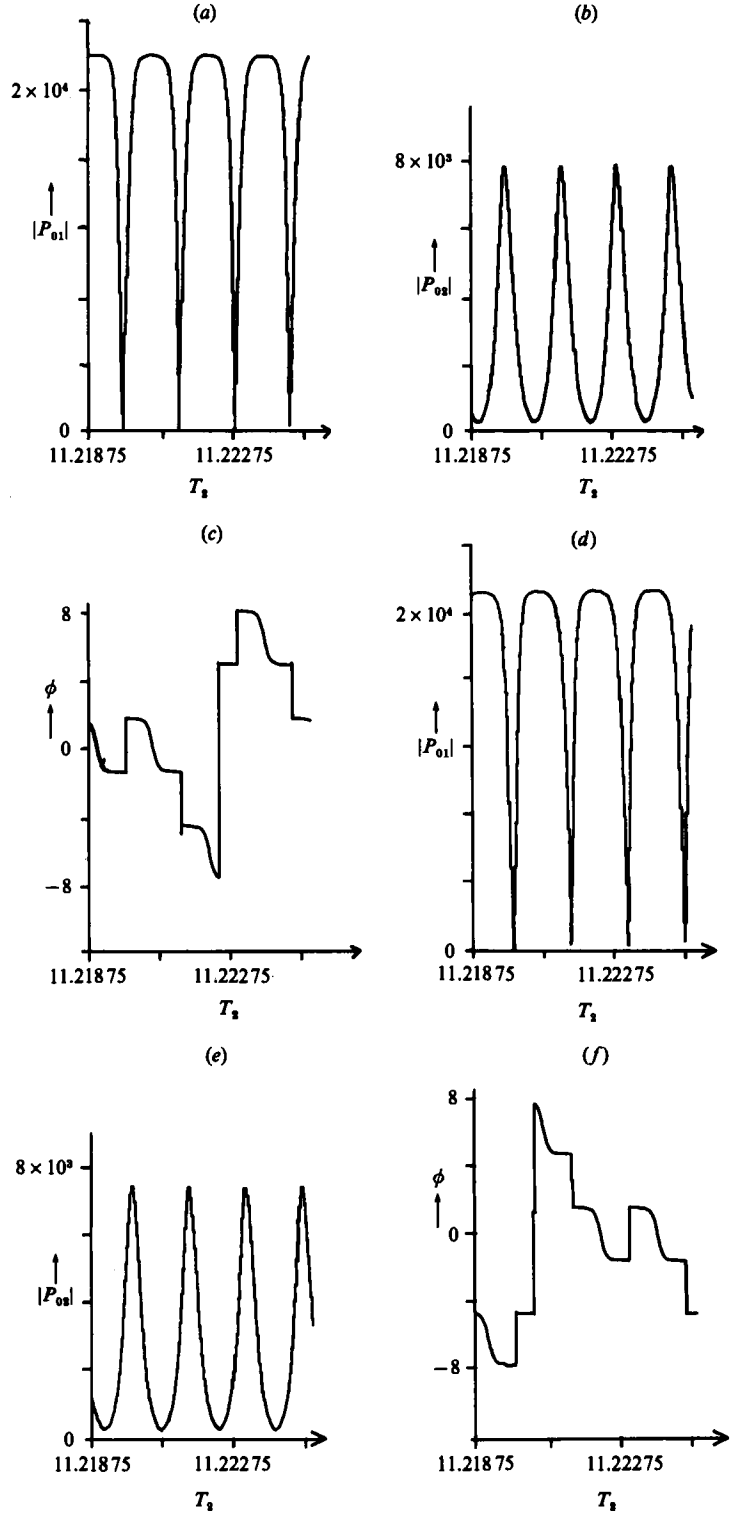

FIGURE 4*a–f*. For caption see next page.

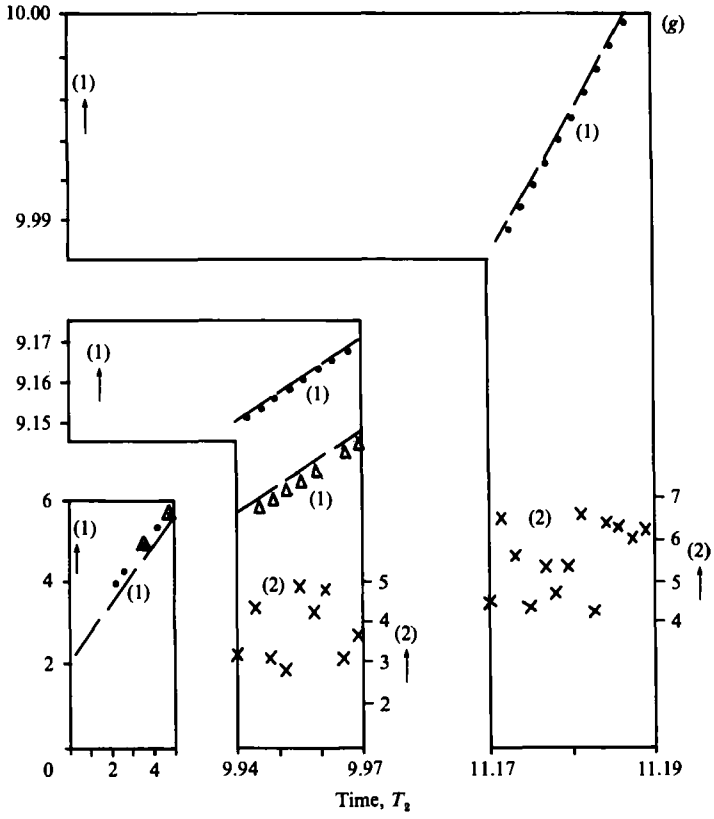

FIGURE 4. Close-up views of computational solutions of the temporal case (3.1), with $P_{03} = P_{02}$. (*a*) $|P_{01}|$; (*b*) $|P_{02}|$; (*c*) phase function ϕ; plot interval is refined to exactly Δ. (*d*), (*e*) and (*f*) are as in (*a*)–(*c*) but with Δ doubled to 0.0000125. Notice that the computed ϕ ($\equiv 2\nu_2 - \nu_1$) jumps by $\pm 2\pi$ or $\pm 4\pi$ whenever the arguments ν_1 or ν_2 are switched through 2π by the machine-based argument function. (*g*) Local maxima and minima of $\ln(|P_{01}|)$ [marked (1), (2) respectively] during three time ranges: results ●, ×, $\Delta = 0.0000125$; △, Δ doubled; ---, the large-time prediction (4.14) for the growth rate. Initial values here are $P_{01,2} = 0,5$.

for (3.1*a*), and similarly for (3.1*b*, *c*); and

$$P_{01}\text{-corr} = \tfrac{1}{2}(P_{01}\text{-pred} + \overline{P_{01}}) + \tfrac{1}{2}\Delta\left[\frac{(1-\mathrm{i})P_{01}\text{-pred}}{\sqrt{2}} - 2\mathrm{i}P_{02}\text{-pred}\,P_{03}\text{-pred}\right], \tag{3.2b}$$

with similar formulae for (3.1*b*, *c*) again. Here $\overline{P_{0n}}$ ($n = 1, 2, 3$) denote the known values at the previous time level.

Representative numerical solutions are presented in figures 2–4. In some of these we took $P_{03} = P_{02}$,† partly to reduce the computational task and partly to compare directly with the analysis of the next section. Throughout, the solutions for P_{01}, P_{02}, P_{03} all develop a highly spiked and erratic appearance, as time T_2 advances, accompanied by fairly rapid growth of the maximum amplitude attained in each spike. The computer plotting of the results had to be done with some care, with regard to the plot density, to capture the spiky behaviour successfully, as the figures

† The same results were obtained, to within machine accuracy, by setting P_{02}, P_{03} equal at time $T_2 = 0$ in the system (3.1*a*–*c*), thus illustrating secondary stability. See also comments in §5.

indicate. [Further results concerning this aspect are given in a 1986 United Tech. Res. Cent., East Hartford, Conn., U.S.A., Report by the authors.] The figures also show the effects of altering the time step Δ, typically about 10^{-5}, which overall seems adequate for determining the trends of the flow solution: see also the later figures.

4. The behaviour at large times/far downstream

To simplify matters here we consider first the case where P_{02} and P_{03} are identical (in fact, this turns out to be almost the general case, at large times, as described at the end of this section). Then, with the definitions

$$P_{01} \equiv R_1 \exp(\mathrm{i}\nu_1), \quad P_{02} = P_{03} \equiv R_2 \exp(\mathrm{i}\nu_2), \quad \phi \equiv 2\nu_2 - \nu_1, \tag{4.1}$$

the governing equations (3.1) reduce to the real coupled system

$$\frac{\mathrm{d}R_1}{\mathrm{d}T_2} = \frac{1}{\sqrt{2}} R_1 + 2R_2^2 \sin\phi, \tag{4.2a}$$

$$\frac{\mathrm{d}R_2}{\mathrm{d}T_2} = \tfrac{1}{2}R_2 - \tfrac{1}{4}R_1 R_2 \sin\phi, \tag{4.2b}$$

$$R_1 \frac{\mathrm{d}\phi}{\mathrm{d}T_2} = (2R_2^2 - \tfrac{1}{2}R_1^2)\cos\phi - \kappa R_1, \tag{4.2c}$$

for the real functions R_1, R_2, ϕ, where $\kappa \equiv (1 - 1/\sqrt{2})$ is positive. A similar simplification occurs if $|P_{02}| = |P_{03}|$.

The aim now is to describe the large-time response of (4.2), or the large-distance response in the spatial case referred to later in §5. The proposal below is that the amplitudes R_1 ($\equiv |P_{01}|$) and R_2 ($\equiv |P_{02}|$) typically then both grow exponentially fast, proportional to $\exp[\sigma T_2]$, say, where σ is an unknown $O(1)$ positive constant, but with an increasingly fast (spiky) dependence on $\exp[\sigma T_2]$ emerging as well. Other asymptotic forms can also be written but generally are unattainable from most initial values, we believe. In particular, a promising account that we tried has $s^{-1}R_1, s^{-1}R_2, \phi$ being dependent only on s at large times, where $s \equiv \exp(\sigma T_2)$; this proved unattainable in general but it did help in pointing to the final proposed form below. The proposal is that the solution settles into a pattern of recycling states (i)–(iv) when $T_2 \gg 1$, as depicted in figure 5.

In the first of the recycling states, (i), the expansions holding are

$$R_1 = s\hat{R}_1(s) + \ldots, \quad R_2 = s\hat{R}_2(s) + \ldots, \quad \phi = \tfrac{1}{2}\pi + s^{-1}\hat{b}(s) + \ldots \quad [s = \exp(\sigma T_2)], \tag{4.3}$$

where an arbitrary multiple of 2π is omitted from ϕ and the constant σ is determined later (see (4.14)). Then (4.2*a–c*) yield the leading-order balances

$$\sigma \frac{\mathrm{d}\hat{R}_1}{\mathrm{d}s} = +2\hat{R}_2^2, \quad \sigma \frac{\mathrm{d}\hat{R}_2}{\mathrm{d}s} = -\tfrac{1}{4}\hat{R}_1 \hat{R}_2, \quad \sigma\hat{R}_1 \frac{\mathrm{d}\hat{b}}{\mathrm{d}s} = -(2\hat{R}_2^2 - \tfrac{1}{2}\hat{R}_1^2)\hat{b} - \kappa\hat{R}_1, \tag{4.4a–c}$$

from which the solutions have the form

$$\hat{R}_1 = \hat{\nu}\tanh(\hat{p}), \quad \hat{R}_2 = \frac{\hat{\nu}}{\sqrt{8}}\operatorname{sech}(\hat{p}), \quad \hat{p} = +\frac{\hat{\nu}}{4\sigma}(s - s_0), \tag{4.5a–c}$$

$$\hat{b} = \{-\hat{B}\cosh^2(\hat{p}) + 2\kappa\hat{\nu}^{-1}\}\coth(\hat{p}), \tag{4.5d}$$

where $\hat{\nu}, s_0, \hat{B}$ are unknown constants and necessarily $\hat{p}$ is positive, as is $\hat{\nu}$. This state, which is predominantly inviscid, persists for all positive $\hat{p}$, except that as $\hat{p} \to \infty$

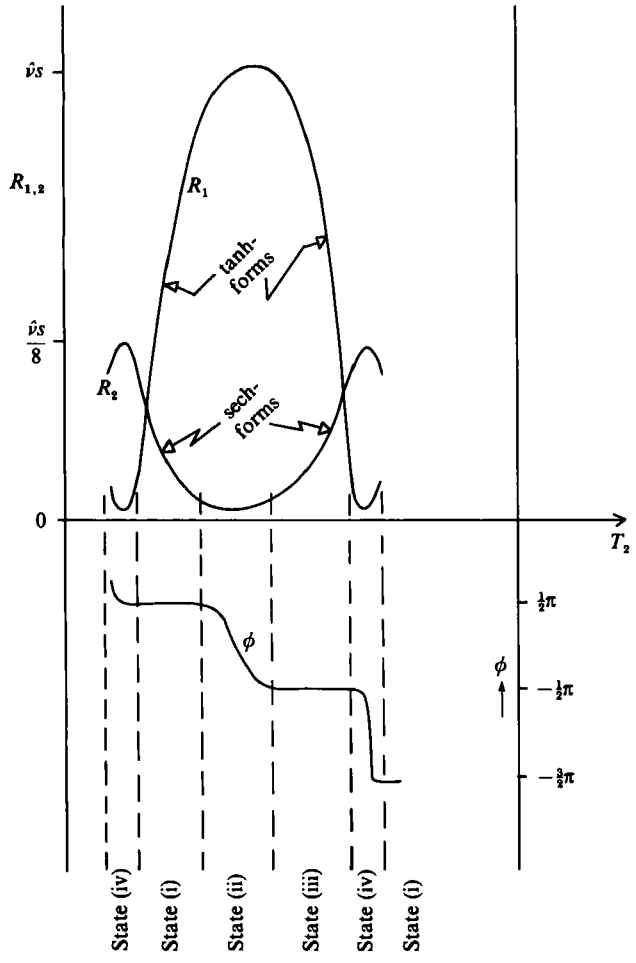

FIGURE 5. Sketch (not to scale) of the cycle of states (i)–(iv) proposed in §4, for large times T_2 or for large distances X_2 in the spatial case referred to in §5 and figure 6 below. The corresponding amplitudes R_1, R_2 and the effective phase ϕ during the re-cycling states are also shown. The maximum values of R_1, R_2 are, in turn, $s\hat{\nu}$ and $s\hat{\nu}/\sqrt{8}$, where $s \equiv \exp(\sigma T_2)$, $\hat{\nu}$ is a positive constant and σ is given in (4.14), cf. figure 4(*a–f*).

(corresponding to *increasing* s and time T_2) $\hat{b}$ grows indefinitely like $-\frac{1}{4}\hat{B}\exp(2\hat{p})$, while $\hat{R}_1 \to \hat{\nu}$ then, and $\hat{R}_2 \to 0$ like $\hat{\nu}\exp(-\hat{p})/\sqrt{2}$. This leads into the next state, (ii).

State (ii), where the phase function ϕ varies by an $O(1)$ amount, has the new expressions

$$R_1 = s\hat{\nu} + \tilde{R}_1(s) + \ldots, \quad R_2 = s^{\frac{1}{2}}\tilde{R}_2(s) + \ldots, \quad \phi = \tilde{a}(s) + \ldots, \tag{4.6}$$

applying for a range $\frac{1}{2}\pi > \tilde{a} > -\frac{1}{2}\pi$, with s increased by a logarithmic factor from its value in state (i). Here R_1, R_2 reach their local maximum and minimum values, respectively, for each spike. The balances from (4.2) are

$$\frac{\sigma\,\mathrm{d}\tilde{R}_1}{\mathrm{d}s} + \left(\sigma - \frac{1}{\sqrt{2}}\right)\hat{\nu} = 2\tilde{R}_2^2\sin(\tilde{a}), \quad \frac{\sigma\,\mathrm{d}\tilde{R}_2}{\mathrm{d}s} = -\tfrac{1}{4}\hat{\nu}\tilde{R}_2\sin(\tilde{a}), \tag{4.7a,b}$$

$$\frac{\sigma\,\mathrm{d}\tilde{a}}{\mathrm{d}s} = -\tfrac{1}{2}\hat{\nu}\cos(\tilde{a}), \tag{4.7c}$$

showing the entrance here of the viscous growth term. Hence we have the solutions (see also figure 5)

$$\tilde{a}(s) = -\tfrac{1}{2}\pi + 2\tan^{-1}\left[\exp\left\{-\frac{\hat{\nu}}{2\sigma}(s-s_1)\right\}\right], \tag{4.8a}$$

$$\tilde{R}_2(s) = \tilde{A}_2|\cos(\tilde{a})|^{-\frac{1}{2}}, \tag{4.8b}$$

$$\tilde{R}_1(s) = -4\tilde{A}_2^2\hat{\nu}^{-1}|\cos(\tilde{a})|^{-1} + (2^{-\frac{1}{2}}-\sigma)\hat{\nu}s\sigma^{-1} + \tilde{B}_1, \tag{4.8c}$$

where $s_1, \tilde{A}_2, \tilde{B}_1$ are constants, with $\tilde{A}_2 > 0$. The match with the previous state (i) above is achieved as $\tilde{a} \to \frac{1}{2}\pi -$, $s - s_1 \to -\infty$, as required, giving $\tilde{R}_{1,2} \to \mp\infty$ in turn and fixing $\tilde{A}_2 = \frac{1}{2}\hat{\nu}$. As s (and T_2) increases now, however, a new state is implied for even larger s, since as $s - s_1 \to +\infty$, $\tilde{R}_{1,2} \to \mp\infty$ again, while the phase function $\tilde{a} \to -\frac{1}{2}\pi$ from above.

The subsequent state, (iii), is therefore similar to the earlier inviscid one (i), with s increased again, but it has

$$R_1 = s\hat{R}_1(s) + \ldots, \quad R_2 = s\hat{R}_2(s) + \ldots, \quad \phi = -\tfrac{1}{2}\pi + s^{-1}\hat{b}(s) + \ldots, \tag{4.9}$$

instead of (4.3), which changes all the signs immediately following the equality signs in (4.4). So here (4.5*a–d*) hold again except that

$$\hat{p} = -\frac{\hat{\nu}}{4\sigma}(s-s_0), \quad \hat{b} = \{-\hat{B}\cosh^2(\hat{p}) - 2\kappa\hat{\nu}^{-1}\}\coth(\hat{p}). \tag{4.10}$$

In consequence the range of increasing s from $-\infty$ here *reduces* $\hat{p}$ from large positive values (where the join with the previous, viscous, state (ii) takes places) to zero+ [at a finite value s_0 of s], whereupon $|\hat{b}| \to \infty$, $\hat{R}_1 \to 0+$ and yet another new state, (iv), comes into play.

During this next state (iv) the amplitudes $R_{1,2}$ acquire their local minima and maxima, respectively, per spike, while the effective phase ϕ decreases from $-\frac{1}{2}\pi$ to $-\frac{3}{2}\pi$. The governing equations (4.2) reduce in essence to the forms

$$\frac{\mathrm{d}R_1}{\mathrm{d}T_2} = \tfrac{1}{4}s_0^2\hat{\nu}^2\sin(\phi), \tag{4.11a}$$

$$\frac{\mathrm{d}R_2}{\mathrm{d}T_2} = -\frac{s_0\hat{\nu}R_1}{4\sqrt{8}}\sin(\phi), \tag{4.11b}$$

$$R_1\frac{\mathrm{d}\phi}{\mathrm{d}T_2} = \tfrac{1}{4}s_0^2\hat{\nu}^2\cos(\phi). \tag{4.11c}$$

Here, since R_2 is $s_0\hat{\nu}/\sqrt{8}$ and large, to leading order, s is close to the value s_0, and $R_1 \ll R_2$. Hence the local solutions are

$$R_1 = A_1|\cos\phi|^{-1}, \tag{4.12a}$$

$$R_2 - \frac{s_0\hat{\nu}}{\sqrt{8}} = C_2 - \frac{s_0^3\hat{\nu}^3(T_2-D_2)^2}{32\sqrt{8}}, \tag{4.12b}$$

$$\phi = -\tan^{-1}\left[\frac{s_0^2\hat{\nu}^2(T_2-D_2)}{4A_1}\right], \tag{4.12c}$$

with $A_1\,(>0)$, C_2, D_2 being constants. The merging with the previous state (iii) above is then achieved as $\phi \uparrow -\frac{1}{2}\pi$, $(T_2-D_2) \to -\infty$, as required, and determines $A_1 = (\nu\hat{B} + 2\kappa)$. As (T_2-D_2) increases R_1, R_2 pass through their minimum and

maximum values, after which, as $(T_2 - D_2) \to +\infty$, R_1 increases indefinitely and R_2 decreases, with ϕ approaching $-\frac{3}{2}\pi$ from above. The solution then moves into the start of state (i) above, with ϕ decreased overall by 2π, and so the cycle continues.

That completes the large-time description, shown in figure 5, apart from the unknown growth factor σ. This is determined from the overall integral constraint

$$[\tfrac{1}{8}R_1^2 + R_2^2] = \int_0^{T_2} \left[\frac{R_1^2}{4\sqrt{2}} + R_2^2\right] \mathrm{d}T_2 + [\tfrac{1}{8}R_1^2(0) + R_2^2(0)] \tag{4.13}$$

derived from the original equations (4.2a, b) by eliminating $\sin\phi$ there. In the large-time cycle the dominant contribution to (4.13) comes from state (i), which to leading order gives $\frac{1}{8}\tilde{\nu}^2 s^2$ on the left-hand side of (4.13) and $\tilde{\nu}^2 s^2 \sqrt{2}/16\sigma$ on the right, for large s. Hence the growth rate is

$$\sigma = 1/\sqrt{2}. \tag{4.14}$$

Another integral constraint should also be mentioned here, namely

$$\frac{R_1 R_2^2 \cos\phi}{(\frac{1}{8}R_1^2 + R_2^2)^{2q}} = \int_0^{T_2} R_1 R_2^2 (\tfrac{1}{8}R_1^2 + R_2^2)^{-2q-1}$$

$$\times \left[\left\{\left(\frac{1}{\sqrt{2}} + 1\right)(\tfrac{1}{8}R_1^2 + R_2^2) - 2q\left(\frac{R_1^2}{4\sqrt{2}} + R_2^2\right)\right\}\cos\phi + \kappa(\tfrac{1}{8}R_1^2 + R_2^2)\sin\phi\right] \mathrm{d}T_2, \tag{4.15}$$

which holds for all $q < \frac{3}{4}$ and brings in (4.2c) as well as (4.2a, b). The earlier studied account, referred to in the second paragraph of this section, turned out to be inconsistent with the combination of (4.13), (4.15), owing to the leading-order terms arising. In contrast, the present proposal based on the states (i)–(iv) is found to be not inconsistent with (4.13), (4.15) because higher-order terms active in the viscous state (ii), for example, allow the extra freedom necessary to satisfy (4.15).

Comparisons between the proposed large-time cycle (i)–(iv) and the computed results of §3 are quite affirmative. Figure 4(*a–f*) shows close-up views of the computations, for two step sizes, over a short interval at large time and the computed behaviour of the amplitudes R_1, R_2 and effective phase ϕ there appears well in line with the envisaged cycle depicted in figure 5. Also, the proposed ratio $\sqrt{8} = 2.828\ldots$ of the maximum values of R_1, R_2 at large times (from (4.5)) is close to the approximate value 2.821 of the ratio computed near time $T_2 = 11.22$ in figure 4(a, b). Again, the plot in figure 4(g) of the maximum values of R_1 and the times at which those maxima are attained, according to the numerical results, seems in accord with the ultimate growth rate of (4.14) as well as with the increasingly fast, exponential, rate at which the proposed cycle repeats itself. The plots of the minima in figure 4(g), and of the corresponding times, are less clear. They appear somewhat chaotic, as do the minima in figures 2 and 3; this may or may not be due solely to the computational difficulty of capturing the minima accurately, since the latter occur extremely sharply (both computationally and in the limiting proposal above) as opposed to the more gradual modulation during the rest of each cycle.

Physically, there are several items of interest to record regarding the large-time cycle (i)–(iv) above. The first is the role of viscosity, through its linear-growth-term contributions proportional to $R_{1,2}$ in (4.2a, b). These contributions remain significant overall at large times since they determine the maximum growth rate of the cycle, i.e. the constant σ in (4.14), despite being negligible in the internal dynamics of most of the cycle (i)–(iv). A similar phenomenon occurs in the companion works of Smith (1986a, b). Further on this point, although the ultimate *large*-scale behaviour (states (i), (iii)) is broadly inviscid in nature, viscous forces are significant in the *small/*

fast-scale responses of states (ii), (iv) which provide a 'rejuvenation' of the nonlinear fundamental and subharmonic components, a rejuvenation which is essential to the continuing development of the flow. Secondly, the maximum growth rate of all the three waves $|P_{01}|, |P_{02}| = |P_{03}|$ of the particular triad studied is $\sigma = 1/\sqrt{2}$, which is also the growth rate of the two-dimensional wave on linear grounds but is greater than the linear growth rate of the three-dimensional waves. This increase of the three-dimensional waves' growth rate, owing to nonlinearity, represents in many senses the most important aspect of the nonlinear triad interaction: see also §5. Thirdly, the cycle proposed above shows a continual interchange and enhancing of energy taking place between the nonlinear modes, as time increases, with R_1, R_2 being comparable in size during states (i), (iii), whereas R_1 is dominant in state (ii) and R_2 is dominant during state (iv), as the effective phase function ϕ continues to fall. Fourthly, the solutions have a very chaotic appearance in some respects but this aspect seems of relatively little significance in the general trend of the solution, certainly compared with the enhanced spikiness which both the calculations and the analytically based cycle (i)–(iv) exhibit. Lastly here, there is the issue of whether the account (i)–(iv) can be generalized to three unequal modes, with $P_{02} \neq P_{03}$: it can, as the Appendix shows. Further comments, and comparisons with experiments, are presented in the next section.

5. Further discussion, and comparisons with experiments

5.1. *General discussion*

A number of comments (I–IV) should be made at this stage. First (Comment I), the resonant-triad three-dimensional interaction studied here arises 'sooner', i.e at lower amplitudes, than most other known types of three-dimensional interactions including those studied by Smith & Burggraf (1985) and Smith (1986*a*, *b*), for a given frequency of the incoming disturbance. This is much as Craik (1971) suggested, and as experiments reveal (see below, particularly §5.2), and it can be seen by comparing the typical pressure amplitude, $O(1)$, of the triad in (2.6*a*) with the higher amplitude, $O(\Omega^{\frac{1}{2}})$, required in (3.2*a*) of Smith (1986*b*), for instance (see also the references just above). So (Comment II) an incoming disturbance of sufficiently small amplitude encounters the triad response, and its enhanced interchanging of energy between modes [§4], ahead of the two-dimensional mechanisms of Smith (1986*a*) or its three-dimensional counterpart in Smith (1986*b*). On the other hand, however (Comment III), the nonlinear growth of the triad is (*a*) not excessive, although still large [§4], and (*b*) almost bound to lead on, downstream, into the type of three-dimensional interaction studied in Smith (1986*b*) as the pressure amplitude rises from $O(1)$ to $O(\Omega^{\frac{1}{2}})$. Moreover (Comment IV), the three-dimensional interaction of the last-named paper then *does* exhibit excessive nonlinear growth [compared with (*a*) above] for oblique angles θ exceeding $\tan^{-1}(\sqrt{2}) = 54.7°$, which includes the three-dimensional parts of the triad [in view of (2.5)] and could therefore accentuate them subsequently. Again (Comment V), an incoming disturbance of amplitude higher than in II above can by-pass the triad stage and enter the first stage [or, come to that, later higher-amplitude stages] of Smith & Burggraf (1985), Smith (1986*a*, *b*) directly. Finally (Comment VI), other points with regard to sublayer bursting, secondary instabilities, the whole ensuing transition process, other starting flows, and further work, are as given in the references above.

Concerning Comment I above, this work fully supports, on a rational basis, Craik's (1971) suggestion of the existence of resonant triads in boundary layers. The only

rider we would add to that statement is this: the coefficients in the governing equations, found in §2, are such that no finite-time breakdown can occur, thus ruling out one of the further suggestions of Craik (1971), so far at least. The situation may be different for other starting flows such as three-dimensional ones or for other frequency regimes. In the meantime, however, we feel that, quite apart from other facets, even the mere testing and verification above of Craik's physically motivated basic idea may add considerably to the value of the structural, and in particular the relatively high-frequency, theory used here and in related studies.

Alternative mechanisms and possibilities do exist, as Smith & Burggraf (1985), Smith (1986*a*, *b*) and others note. These include the three-dimensional nonlinear interaction referred to in Comments I–V above; Herbert's (1984*a*, *b*) suggested secondary instabilities and/or Squire modes, although these appear to have no rational basis so far and the distinction from the triad interaction for example is not yet clear; multiple-mode interactions; higher-amplitude phenomena; and the alternative upper-branch type of scalings and processes, e.g. Gajjar & Smith (1985).

Even within the context of resonant triads alone, there are still many further developments to be explored. For example, the solutions in §§3 and 4 and the Appendix are solely for the time-dependent problem, in (3.1); what happens for purely spatial dependence? To be sure, if only streamwise X_2 dependence is present in (2.31) then virtually the same results can be expected to hold, because of the signs in (2.31). Computations in this simplest spatial case, i.e. for the triad equations

$$\left.\begin{aligned} 2\frac{\mathrm{d}P_{01}}{\mathrm{d}X_2} &= \frac{1}{\sqrt{2}}(1-\mathrm{i})P_{01}-2\mathrm{i}P_{02}P_{03}, \\ \frac{5}{4}\frac{\mathrm{d}P_{02}}{\mathrm{d}X_2} &= \tfrac{1}{2}(1-\mathrm{i})P_{02}-\tfrac{1}{4}\mathrm{i}P_{01}P_{03}^{*}, \\ \frac{5}{4}\frac{\mathrm{d}P_{03}}{\mathrm{d}X_2} &= \tfrac{1}{2}(1-\mathrm{i})P_{03}-\tfrac{1}{4}\mathrm{i}P_{01}P_{02}^{*}, \end{aligned}\right\} \tag{5.1}$$

seem to confirm the expectation, as shown in figure 6 where the spiky growing response produced downstream for large X_2 is analogous to that in the previous temporal cases and the nonlinear growth falls into line with the analogue of the result (4.14). For interest, figure 6 also shows the effects of a small change in the starting conditions. In keeping with the asymptotics of §4, there is some sensitivity to the starting conditions in absolute terms, and this becomes more pronounced as time or distance increases, inducing an enlarged shift of the solution, but the sensitivity is still relatively (and qualitatively) small since the overall solution is growing exponentially in any case. With pure cross-stream (Z_2) dependence, in contrast, a rather different coupled form comes out of (2.31), namely

$$\frac{\sqrt{3}}{4}\frac{\mathrm{d}P_{02}}{\mathrm{d}Z_2} = \tfrac{1}{2}(1-\mathrm{i})P_{02}+\frac{(1+\mathrm{i})P_{02}|P_{03}|^2}{2\sqrt{2}}, \tag{5.2a}$$

$$-\frac{\sqrt{3}}{4}\frac{\mathrm{d}P_{03}}{\mathrm{d}Z_2} = \tfrac{1}{2}(1-\mathrm{i})P_{03}+\frac{(1+\mathrm{i})P_{03}|P_{02}|^2}{2\sqrt{2}}, \tag{5.2b}$$

which has still to be investigated. Also, oblique waves dependent on a linear combination $(\overline{\alpha}_2 X_2+\overline{\beta}_2 Z_2-\overline{\Omega}_2 T_2)$, say, need further study, although here on physical grounds the group velocity represented by the coefficients on the left-hand side of (2.31) imposes restrictions on the constants $\overline{\alpha}_2, \overline{\beta}_2, \overline{\Omega}_2$, which, as before, rule out the occurrence of finite-time singularities. Another matter is the phenomenon of

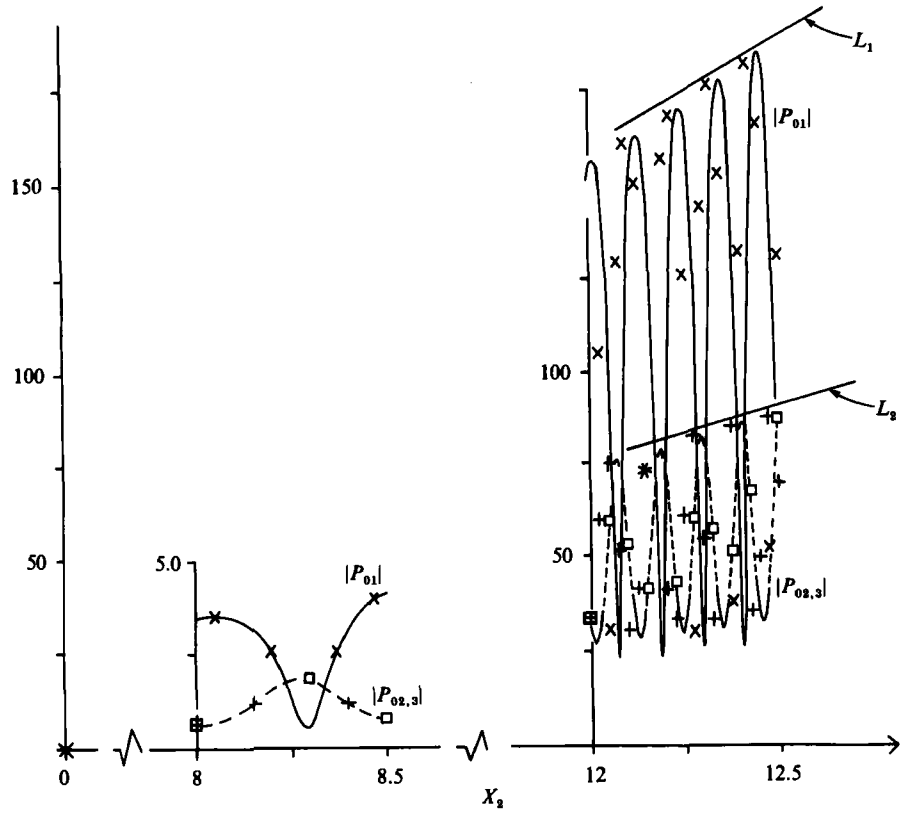

FIGURE 6. Two computational solutions of the purely spatial case (5.1), plotted versus X_2: for $P_{01,2,3} = 1+\mathrm{i}, 0.5, 0.49$ at $X_2 = 0$, ——, P_{01}; – – –, P_{03}, □, P_{02}: for $P_{01,2,3} = 1+\mathrm{i}, 0.5, 0.5$ at $X_2 = 0$, ×, P_{01}; +, P_{03}; +, P_{02}. Also shown for comparison, as curves L_1, L_2, are the predicted exponential growths $\exp(X_2/2\sqrt{2})$ from the spatial analogue of the result (4.14) for large distances downstream.

'detuning', referred to in the experiments of Saric *et al.* (1984) and in private communications with Dr A. D. D. Craik (1985), associated with a slight difference $\Delta\Omega$ between the incident frequency and the exact value for resonance taken in §2. In the context of multiple scales this can be accommodated to some extent by considering disturbances proportional to $\exp(-\mathrm{i}\Omega_2 T_2)$, times functions of X_2, say, in (2.31), with the constant Ω_2 representing the detuning $\Delta\Omega$. There are various generalizations or alternative cases of detuning. One example is for disturbances proportional to $\exp(\mathrm{i}\alpha_2 X_2 + \mathrm{i}\beta_2 T_2)$ where, in effect, (2.31*a–c*) reduce to the nonlinear ordinary differential system

$$\frac{\mathrm{d}P_{01}}{\mathrm{d}T_2} = \left(\frac{1}{\sqrt{2}} - \frac{\mathrm{i}}{\sqrt{2}} - 2\mathrm{i}\alpha_2\right) P_{01} - 2\mathrm{i}P_{02}P_{03}, \tag{5.3a}$$

$$\frac{\mathrm{d}P_{02}}{\mathrm{d}T_2} = \left(\tfrac{1}{2} - \tfrac{1}{2}\mathrm{i} - \tfrac{5}{4}\mathrm{i}\alpha_2 - \frac{\sqrt{3}}{4}\mathrm{i}\beta_2\right) P_{02} - \tfrac{1}{4}\mathrm{i}P_{01}P_{03}^*, \tag{5.3b}$$

$$\frac{\mathrm{d}P_{03}}{\mathrm{d}T_2} = \left(\tfrac{1}{2} - \tfrac{1}{2}\mathrm{i} - \tfrac{5}{4}\mathrm{i}\alpha_2 + \frac{\sqrt{3}}{4}\mathrm{i}\beta_2\right) P_{03} - \tfrac{1}{4}\mathrm{i}P_{01}P_{02}^*. \tag{5.3c}$$

This is also discussed in the Appendix. Still more general are the partial differential systems for initial-value or forced problems, where (e.g.) P_{01}, P_{02}, P_{03} in (2.31) are

specified as functions of X_2 and/or Z_2 initially. Here preliminary calculations by the current authors, for the case of X_2, T_2 dependence being present, showed a two-humped form tending to emerge downstream as time increases (see also Kaup, Riemann & Bers (1979), Kaup (1981), Wersinger, Finn & Ott (1980) – references which were kindly pointed out to us by Dr A. D. D. Craik – and Craik (1985), Weiland & Wilhelmsson (1977) and references therein) but with substantial growth and spikiness also occurring, much as in §§3 and 4. A further extension to three three-dimensional waves, rather than the two-dimensional-plus-two-three-dimensional coupling in (2.3), is also of interest. Extra scales intermediate between $(T_0 X_0, Z_0)$ and (T_2, X_2, Z_2) in (2.1), which arise in the studies by Smith & Burggraf (1985), Smith (1986*a*, *b*), do not seem relevant here, however. Throughout all these extensions of the present study, a major question to be answered (see also the Appendix) concerns the nonlinear growth rates: can they exceed that found in §4? And, whether the answer is 'yes' or 'no', what happens afterwards?

What happens afterwards can be anticipated reasonably well for special cases like those in §§3 and 4 and the Appendix, in fact. The higher-amplitude stage (called stage 1) discussed in the three last-named references comes into operation next, as indicated in our earlier Comments (II)–(IV), but with three three-dimensional modes present. For, from §4, each mode in the triad grows typically like $\exp(\sigma T_2)$ in amplitude, accompanied by the spiky and significant contracting proportional to $\exp(\sigma T_2)$ in its temporal scale. So (Comment VII), when $\exp(\sigma T_2) \to O(\Omega^{\frac{1}{2}})$, i.e. at the later time

$$T_2 \sim (2\sigma)^{-1} \ln \Omega, \tag{5.4}$$

the so-called stage 1 of the three references immediately above is encountered, because of the pressure rise; and meanwhile the current two timescales $(T_0, T_2) \equiv (\Omega T, T)$ in (2.1) split into three $(T_0, T_1, T_2) \equiv (\Omega T, \Omega^{\frac{1}{2}} T, T)$, exactly as required for that stage 1. Other frequency domains (e.g. $\Omega \to Re^{\frac{1}{4}}$) and/or increased distance downstream may lead on to later stages of transition, perhaps the most significant subsequent stage being the Euler stage of length- and timescales $O(Re^{-\frac{1}{2}})$, to which all eventual growth mechanisms, be they two- or three-dimensional, secondary or inflexional, appear to lead.

5.2. *Comparisons with experiments*

Finally, let us compare the above theoretical picture, and especially the Comments (I)–(VII), with the recent experimental findings, particularly those of Saric *et al.* (1984) and Kachanov & Levchenko (1984). The stations at which resonant triads and other significant three-dimensional action are first found to arise experimentally are indicated in figure 4 of Saric *et al.*, for example, and are quite well beyond the lower-branch neutral curve, in line with the present high-frequency assumption. There is clear evidence then of subharmonic growth. Saric *et al.*'s figures 1–3 and subsequent ones show also a 'window' effect for the occurrence of the triad [here see also the recent computations by Herbert (1984*a*, *b*) and Malik (1986)], with the successive input of disturbance sizes of 0.3 %, 0.4 % and 1 % producing, in turn, so-called C-type, H-type and K-type responses [after Craik, Herbert and Klebanoff (Klebanoff, Tidstrom & Sargent 1962) respectively]. This tends to provide good experimental confirmation of the successive/increased-amplitude processes envisaged theoretically in Comments (I)–(VII) above, since we would indeed associate the C-type response with the present study (pressure amplitude of $O(1)$); then perhaps associate the H-type response with the next stage 1 of Smith & Burggraf and Smith (1986*a*, *b*), with the pressure amplitude raised to $O(\Omega^{\frac{1}{2}})$ [note, however, the reservations at

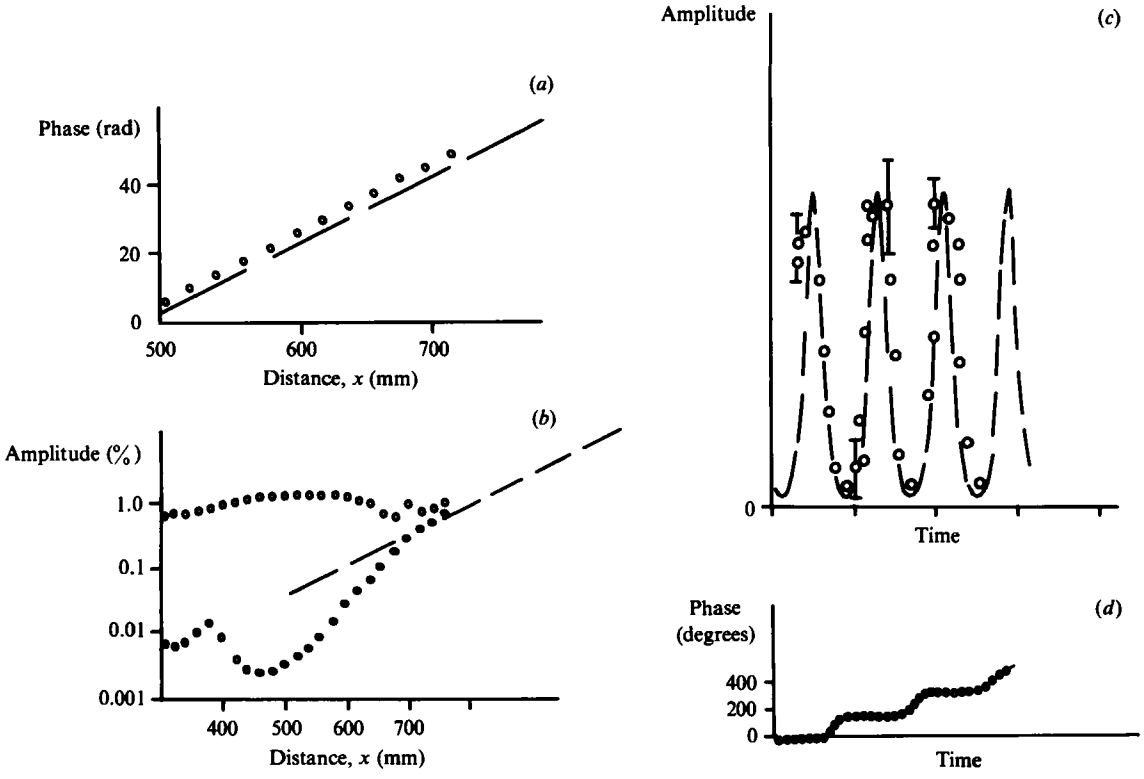

FIGURE 7. Comparisons with the (nonlinear) experiments of Kachanov & Levchenko (1984). (*a*), (*b*) The growths [versus distance x] of phase and amplitude for the fundamental and subharmonic components: ○○○○ (fundamental), ●●●● (subharmonic) experiments; – – –, theory, from (4.14) combined with the triple-deck scalings. (*c*), (*d*) compare representative experimental values (○○○○, with typical scatter/reading error shown I) of the subharmonic amplitude and phase with the theory (——), versus normalized/slow time, using figure 17 (*b*) of Kachanov & Levchenko (1984) and figures 4(*c*), 4(*f*), 5 of the present paper.

present with respect to the H-type interaction in an earlier paragraph]; and then associate the K-type response with the subsequent stage 2 (pressure amplitude raised to $O(\Omega)$) or Euler stage of the last three references above. Again, the increased growth observed in the three-dimensional component during the C-type response, e.g. in figure 9 of Saric *et al.*, is not inconsistent with the theoretical prediction (4.14) of a relative increase by a factor of $\sqrt{2}$. Finally here, the wave angle θ at which the C-type behaviour is observed is quoted as 53–63° by Saric *et al.* (including the experiments of Kachanov & Levchenko (1982) and Saric & Thomas (1984)), which ties in reasonably well with the predicted angle of 60° in (2.5): see also Smith & Burggraf and Smith (1986*a*, *b*).

In more detail, and concerning now the experiments of Kachanov & Levchenko (1984), more quantitative agreement with the theory is found. First, there is good broad agreement with all of the main figures 5–10, 12, 13, 15, 17, 20–23 of Kachanov & Levchenko (1984) as regards the phases and amplitudes of the two- and three-dimensional components, whether for free (natural) or forced (controlled) subharmonics upstream. Secondly, many of the remarks made by Kachanov & Levchenko (1984) accord with the theory: thus (on their page 216) 'a subharmonic amplitude changes continuously and its phase remains practically constant between its 180°

jumps. The phase jumps take place when the amplitude crosses the zero value', cf. §4; and (their page 224) 'a practically exponential growth of the subharmonic amplitude is observed, the amplification rates being much larger than those in the linear theory', cf. §4; later (on their page 224). 'Then...large deviations of fundamental wave amplification rate from a linear law and a large deformation...are observed, which indicates the onset of the breakdown of the laminar regime', cf. Comments III–V, VII of this section. Thirdly, Kachanov & Levchenko (1984) (pp. 221, 235) record a typical wave angle of approximately 63° for resonance, relatively close to the prediction (2.5) of 60° (and relatively far from the alternative theoretical predictions noted on their page 221). Our figure 7 (a, b) compares the experimentally observed growths of the phase and amplitude of the two- and three-dimensional components [from Kachanov & Levchenko (1984), figures 10, 13] with the theoretical result given in (4.14) for the ultimate growth. The quantitative agreement in the behaviour downstream is encouraging. Moreover, a closer smaller-scale comparison between the experimental measurements of amplitude and phase, and the corresponding theoretical findings from §§3 and 4, is also presented in figure 7 (c, d). The agreement again seems favourable. In addition we notice how, in the experiments, the times of relatively rapid change in phase correspond well with the times at which the subharmonic amplitude reaches a local minimum; this is as the theory (§4 and figures 4 and 5) predicts. Overall, therefore, both large- and small-scale comparisons between the theory and the experiments appear quite encouraging indeed.

The interest, comments and encouragement of Drs M. J. Werle, J. E. Carter, M. Gaster, A. D. D. Craik, M. Blair and R. E. Whitehead are gratefully acknowledged, as are the referees' comments. Support for F.T.S. as a consultant with United Technologies Research Center was kindly provided by the UT independent research program and by the US Office of Naval Research.

Appendix. Generalizing the limiting form of §4

In §4 it was assumed for convenience that $P_{03} \equiv P_{02}$. So in this Appendix the general case (3.1) where $P_{03} \not\equiv P_{02}$ is considered, for large times, and the extra effects of detuning as represented by (5.3) are also incorporated. In (5.3) we put

$$P_{0n} = R_n \exp(\mathrm{i}\nu_n), \quad \text{for } n = 1,2,3; \quad \phi = \nu_2 + \nu_3 - \nu_1; \tag{A 1}$$

and then the nonlinear equations (with $' \equiv \mathrm{d}/\mathrm{d}T_2$)

$$R_1' = \frac{R_1}{\sqrt{2}} + 2R_2 R_3 \sin\phi, \tag{A 2}$$

$$R_2' = \tfrac{1}{2}R_2 - \tfrac{1}{4}R_1 R_3 \sin\phi, \tag{A 3}$$

$$R_3' = \tfrac{1}{2}R_3 - \tfrac{1}{4}R_1 R_2 \sin\phi, \tag{A 4}$$

$$R_1 \phi' = \left[2R_2 R_3 - \frac{(R_2^2 + R_3^2) R_1^2}{4R_2 R_3}\right] \cos\phi - \overline{\Gamma} R_1 \tag{A 5}$$

govern the real functions R_n, ϕ. Here $\overline{\Gamma} \equiv \kappa + \frac{1}{2}\alpha_2$.

Our first attempt at generalization took $\hat{R}_3$ ($\approx s^{-1}R_3$) to be different from $\hat{R}_2$ in (4.3) and (4.9), during states (i) and (iii), and indeed an apparently self-consistent

account can then be constructed. However, the initial-value problem suggests otherwise, in fact, since the integral constraint

$$\left.\begin{aligned} R_2^2 - R_3^2 &= A^* \exp(T_2), \\ A^* &\equiv R_2^2(0) - R_3^2(0) \end{aligned}\right\} \quad \text{(A 6)}$$

where

holds from (A 3) and (A 4). This simplifies matters because it requires the difference between R_2^2 and R_3^2 to be no more than $O[\exp(T_2)]$. Therefore, as $R_{2,3}^2$ in (4.3), (4.9) are typically $O[\exp(2\sigma T_2)]$ and so are larger than $O[\exp(T_2)]$, it follows that the states (i) and (iii), as described by (4.3)–(4.5), (4.9)–(4.10) with $\overline{\Gamma}$ replacing κ, remain essentially intact to leading order, and $\hat{R}_3 \equiv \hat{R}_2$, even in the present generalized version. Here (4.14) still fixes σ, the growth rate. The same considerations apply to state (iv) since there $R_{2,3}$ [in (4.11)] are both so large that again the right-hand side of (A 6) is negligible to leading order. Only state (ii) of the cycle is altered much.

State (ii) occurs sooner now, namely when $R_{2,3}$ both fall to $O[\exp(\frac{1}{2}T_2)]$ and the right-hand side of (A 6) comes into operation. Now we have effectively

$$R_1 = s\hat{\nu} + s^{2\sigma-1}\tilde{R}_1, \quad R_{2,3} = s^{\sigma}\tilde{R}_{2,3}, \quad \phi = O(1), \tag{A 7}$$

in place of (4.6). So the governing equations for state (ii) are

$$\sigma\frac{\mathrm{d}\tilde{R}_1}{\mathrm{d}s} = 2\tilde{R}_2\tilde{R}_3\sin\phi, \quad \sigma\frac{\mathrm{d}\tilde{R}_{2,3}}{\mathrm{d}s} = -\tfrac{1}{4}\hat{\nu}\tilde{R}_{3,2}\sin\phi, \quad \sigma\frac{\mathrm{d}\phi}{\mathrm{d}s} = -\tfrac{1}{4}\hat{\nu}\left(\frac{\tilde{R}_2^2+\tilde{R}_3^2}{\tilde{R}_2\tilde{R}_3}\right)\cos\phi, \tag{A 8}$$

and the constraint (A 6) requires

$$\tilde{R}_2^2 - \tilde{R}_3^2 = A^*. \tag{A 9}$$

The solution of (A 8) can be written in the form

$$\tilde{R}_2(s) = \tilde{C}_3\cosh(\tilde{p}), \tag{A 10}$$

$$\tilde{R}_3(s) = \tilde{C}_3\sinh(\tilde{p}), \tag{A 11}$$

$$\cos(\phi(s)) = \tilde{B}_2\,\mathrm{cosech}(2\tilde{p}), \tag{A 12}$$

$$\tilde{R}_1(s) = \tilde{F}_1 - \frac{4\tilde{C}_3^2}{\hat{\nu}}\sinh^2(\tilde{p}), \tag{A 13}$$

where

$$\tilde{p} \equiv \tfrac{1}{2}\cosh^{-1}\left[(1+\tilde{B}_2^2)^{\frac{1}{2}}\cosh\left(\frac{\hat{\nu}}{2\sigma}(s-s_2)\right)\right] \tag{A 14}$$

is positive, $\tilde{C}_3, \tilde{B}_2, \tilde{F}_1, s_2$ are constants, $\tilde{B}_2 > 0$, and $C_3^2 = A^*$. Matching with state (i) is achieved as $\phi \to \frac{1}{2}\pi-$, $s \to -\infty$, with $\tilde{p} \to \infty$, $\tilde{R}_{2,3} \to \infty$ and the difference between $\tilde{R}_2, \tilde{R}_3$ becomes negligible then, in line with our earlier remarks. At the other extreme, $\phi \to -\frac{1}{2}\pi$, $s \to \infty$ and $\tilde{p}, \tilde{R}_{2,3}$ behave similarly to the previous limit, so leading on to state (iii). During state (ii), therefore, $R_{2,3}$ reach their minimum values of order $\exp(\frac{1}{2}T_2)$ and R_1 attains its maximum value.

The altered state (ii) above seems to tie in with the calculation in figure 2, given that in the calculation the value of C_3 is $\sqrt{24}$. The maximum values of $R_{2,3}$ per spike are coming closer together as time increases, subject to the quite large correction of $24\exp(T_2)$ in the difference of the squares.

The detuning present can have only one main effect, we note, for κ in (4.4)–(4.5)

and (4.10) is replaced by $\bar{\Gamma}$. Hence it is possible for certain detunings to restrict the range of the effective phase ϕ by means of the alterations to (4.5) and (4.10). This seems a relatively minor aspect here, however. Overall, the account in §4 is altered little in the general case of (3.1) or (5.3), and in particular the result (4.14) for the growth rate continues to hold.

REFERENCES

Craik, A. D. D. 1971 *J. Fluid Mech.* **50**, 393.

Craik, A. D. D. 1978 *Proc. R. Soc. Lond.* A **363**, 257.

Craik, A. D. D. 1985 *Proc. IUTAM Symp. on Laminar–Turbulent Transition, 1984, Novosibirsk, USSR* (ed. V. V. Kozlov). Springer.

Gajjar, J. & Smith, F. T. 1985 *J. Fluid Mech.* **157**, 53.

Goldstein, M. E. 1985 *J. Fluid Mech.* **154**, 509.

Herbert, T. 1984*a* *AIAA paper no.* 84-0009, presented at Reno, Nevada, Jan. 1984.

Herbert, T. 1984*b* *Proc. IUTAM Symp. on Turbulent and Chaotic Phenomena in Fluids, Kyoto, Japan, Sept. 1983.*

Kachanov, Yu. S. & Levchenko, V. Ya. 1982 *Paper no.* 10-82, ITAM, USSR Acad. of Sci., Novosibirsk.

Kachanov, Yu. S. & Levchenko, V. Ya. 1984 *J. Fluid Mech.* **138**, 209.

Kaup, D. J. 1981 *J. Math. Phys.* **22**, 1176.

Kaup, D. J., Riemann, A. & Bers, A. 1979 *Rev. Mod. Phys.* **51**, 275.

Klebanoff, P. S., Tidstrom, K. D. & Sargent, L. M. 1962 *J. Fluid Mech.* **12**, 1.

Malik, M. R. 1986 *AIAA paper no.* 86-1129, presented at Atlanta, GA, U.S.A., May 12–14, 1986.

Pedley, T. J. & Stephanoff, K. D. 1985 *J. Fluid Mech.* **160**, 337.

Raetz, G. S. 1959 *Northrop Rep.* NOR-59.383 (BLC-121).

Saric, W. S., Kozlov, V. V. & Levchenko, V. Ya. 1984 *AIAA paper no.* 84-0007, presented at Reno, Nevada, Jan. 1984.

Saric, W. S. & Thomas, A. S. W. 1984 *Proc. IUTAM Symp. on Turbulent and Chaotic Phenomena in Fluids, Kyoto, Japan, Sept. 1983.*

Smith, F. T. 1979 *Proc. R. Soc. Lond.* A **366**, 91.

Smith, F. T. 1986*a* *Utd. Tech. Res. Cent., E. Hartford, Conn., Rep. UTRC*-85-36; also *J. Fluid Mech.* **169**, 353.

Smith, F. T. 1986*b* *Utd. Tech. Res. Cent., E. Hartford, Conn., Rep.* UTRC-86-10.

Smith, F. T. & Burggraf, O. R. 1985 *Proc. R. Soc. Lond.* A **399**, 25.

Smith, F. T., Papageorgiou, D. & Elliott, J. W. 1984 *J. Fluid Mech.* **146**, 313.

Usher, J. R. & Craik, A. D. D. 1975 *J. Fluid Mech.* **70**, 437.

Volodin, A. G. & Zelman, M. B. 1978 *Izv. Akad. Nauk. SSSR, Mekh. Zhid. i Gaza* **5**, 78.

Weiland, J. & Wilhelmsson, H. 1977 *Coherent Nonlinear Interaction of Waves in Plasmas.* Pergamon.

Wersinger, J.-M., Fin, J. M. & Ott, E. 1980 *Phys. Fluids* **23**, 1142.